The intellectual disability PAK3 R67C mutation impacts cognitive functions and adult hippocampal neurogenesis

Charlotte Castillon, Laurine Gonzalez, Florence Domenichini, Sandrine Guyon, Kévin da Silva, Christelle M. Durand, Philippe Lestaevel, Cyrille Vaillend, Serge Laroche, Jean-Vianney Barnier, et al.

The intellectual disability *PAK3* R67C mutation impacts cognitive functions and adult hippocampal neurogenesis

Charlotte Castillon[1], Laurine Gonzalez[1], Florence Domenichini[1], Sandrine Guyon[1], Kevin Da Silva[1], Christelle Durand[2], Philippe Lestaevel[2], Cyrille Vaillend[1], Serge Laroche[1], Jean-Vianney Barnier[1*], Roseline Poirier[1*]

[1] Paris-Saclay Neuroscience Institute (Neuro-PSI), UMR 9197, CNRS, Univ. Paris-Sud, Univ. Paris-Saclay, F-91405 Orsay, France;

[2] Institute for Radiological Protection and Nuclear Safety (IRSN), Research department on the Biological and Health Effects of Ionizing Radiation (SESANE), Laboratory of experimental Radiotoxicology and Radiobiology (LRTOX), 92260 Fontenay-aux-Roses, France.

* Correspondence to:

Dr. Roseline Poirier and Dr. Jean-Vianney Barnier, Paris-Saclay Neuroscience Institute, UMR 9197, CNRS, Univ. Paris-Sud, Univ. Paris-Saclay, F-91405 Orsay, France. E-mails: roseline.poirier@u-psud.fr and jean-vianney.barnier@u-psud.fr

Abstract

The link between mutations associated with intellectual disability (ID) and the mechanisms underlying cognitive dysfunctions remains largely unknown. Here, we focused on PAK3, a serine/threonine kinase whose gene mutations cause X-linked ID. We generated a new mutant mouse model bearing the missense R67C mutation of the *Pak3* gene (*Pak3*-R67C), known to cause moderate to severe ID in humans without other clinical signs and investigated hippocampal-dependent memory and adult hippocampal neurogenesis. Adult male *Pak3*-R67C mice exhibited selective impairments in long-term spatial memory and pattern separation function, suggestive of altered hippocampal neurogenesis. A delayed-non-matching-to-place paradigm testing memory flexibility and proactive interference, reported here as being adult neurogenesis-dependent, revealed a hypersensitivity to high interference in *Pak3*-R67C mice. Analyzing adult hippocampal neurogenesis in *Pak3*-R67C mice reveals no alteration in the first steps of adult neurogenesis, but an accelerated death of a population of adult-born neurons during the critical period of 18-28 days after their birth. We then investigated the recruitment of hippocampal adult-born neurons after spatial memory recall. Post-recall activation of mature dentate granule cells in *Pak3*-R67C mice was unaffected, but a complete failure of activation of young DCX^+ newborn neurons was found, suggesting they were not recruited during the memory task. Decreased expression of the KCC2b chloride co-transporter and altered dendritic development indicate that young adult-born neurons are not fully functional in *Pak3*-R67C mice. We suggest that these defects in the dynamics and learning-associated recruitment of newborn hippocampal neurons may contribute to the selective cognitive deficits observed in this mouse model of ID.

Introduction

Intellectual disability (ID) is characterized by impaired cognitive functions and adaptive behaviors (1). Although the causes of ID are highly heterogeneous, genetic factors take a large part in the etiology of ID and numerous cases are caused by mutations in genes located on the X chromosome (2). The proteins encoded by ID genes regulate diverse cellular processes including neurogenesis, neuronal

migration, synaptic function, and regulation of transcription and translation (3, 4). While abnormalities in synaptic plasticity and dendritic spine morphogenesis have been reported to contribute to cognitive deficiencies in models of ID, alterations in different steps of adult hippocampal neurogenesis have also been linked to cognitive deficits in several models of syndromic ID. For example, selective alterations of proliferation, differentiation, neuronal maturation and survival of adult born neurons or defects in their integration into brain networks have been reported in animal models of ID that display cognitive deficits (5). Few recent data also concur in reinforcing this link between gene mutations leading to ID and dysfunction in adult hippocampal neurogenesis (6, 7, 8, 9). To further investigate this issue, we chose as a case study the X-linked p21-activated kinase-3 (PAK3) gene whose reported mutations result in mild to severe ID (10,11,12).

The *Pak3* gene is evolutionary conserved among vertebrates and belongs to group-I PAK family of serine/threonine kinases. PAK3 is highly expressed in brain, in particular in cortex and hippocampus (13). At the cellular level, PAK3 is a downstream effector of the small Rho-GTPases Rac1 and Cdc42 (14). It has been implicated in the LIM kinase pathway that controls actin cytoskeleton dynamics, in the MAP kinase activation and in AMPA-receptor trafficking, mechanisms that play major roles in synaptic plasticity and learning and memory (13, 15, 16). Functionally, genetic invalidation of the *Pak3* gene in mice is associated with selective deficits in hippocampal synaptic plasticity and reduced CREB phosphorylation in cortex and hippocampus (17). PAK3 was also identified as an important player in distinct cellular processes such as in the control of cell cycle exit and differentiation of neuronal precursors in Xenopus embryos (18), in the differentiation of oligodendrocyte precursors (19) and in the time course of interneuron migration during cortical ontogenesis (20).

To date, no study has as yet explored these cellular processes in the adult *in vivo*. Here, we hypothesized that specific ID mutations leading to PAK3 dysfunction may alter adult hippocampal neurogenesis and neurogenesis-dependent cognitive functions. We therefore generated a novel mouse model of *Pak3*-dependent ID by knocking-in the R67C missense mutation (*Pak3*-R67C mouse), strictly identical to the human mutation responsible for moderate to severe non-syndromic ID (21, 22). This mutation changes arginine 67 to a cysteine residue in the regulatory domain of PAK3 in

proximity to the p21 GTPase-binding domain. This mutation decreases the binding of PAK3 to Cdc42 while increasing its binding to Rac1 (23). We characterized the behavioral phenotype of this novel ID model and focused, in particular, on adult neurogenesis-dependent tasks, assessing spatial memory and pattern separation function. We then examined whether the R67C mutation affects any of the key steps of basal adult hippocampal neurogenesis by assessing progenitor cell proliferation, differentiation and survival of adult-born neurons. Finally, we explored adult hippocampal neurogenesis in relation to spatial learning by analyzing the effect of the mutation on neuronal survival and the recruitment of newborn neurons by learning.

Results

Generation of the *Pak3*-R67C mouse model and hippocampus expression of PAK3

To provide insights into the effects of the *Pak3*-R67C mutation, we generated a knock-in mouse model expressing the mutated *Pak3* gene encoding the PAK3-R67C protein. The generation of *Pak3*-R67C mice was done by mutagenesis of the CGC>TGC mutation in the sequence of the second coding exon in the recombination vector (Fig. 1A). We verified that the H*haI* site suppressed by this mutation (22) was absent from the genomic fragment of transgenic males (Fig. 1B). The genomic mutated sequence of exon 2 was confirmed by cloning (data not shown). The mutated allele segregated with Mendelian ratio and mutated hemizygous males and homozygous females were viable and fertile, with normal life span. Mutated hemizygous males and their WT littermate reached adulthood at a normal weight (*Pak3*-R67C mice: 28.44g ± 0.475, n=9; WT: 28.11g ± 0.633, n=9). PAK3 mRNAs were transcribed at a similar level in brain from transgenic and WT adult males as verified by quantitative RT-PCR (data not shown). As shown by western blotting experiments, the PAK3-R67C protein was detected in adult whole brains extracts from transgenic mice (R67C) as a band of similar molecular weight compared to WT mice (Fig. 1C). The expression of the mutated protein was found to be similar to that of the WT protein, as quantified by western blot (Fig. 1C, mean relative PAK3-R67C protein expression compared to WT expression after normalization to β-Actin: 113.3 ± 8.3, n= 3). In brain

structures, PAK3 expression has been broadly reported in hippocampus (24), a structure known to play an important role in cognitive functions. However, to define more precisely its expression in hippocampal subfields (CA1, CA3 and dentate gyrus (DG) and to overcome the lack of specific anti-PAK3 antibodies suitable for immunofluorescence studies, we used *Pak3*-tm1b mice to analyze the expression of β-galactosidase as a reporter of PAK3 promoter activation (25). Free-floating sections from transgenic male brains were stained and we determined hippocampal expression patterns of PAK3. We observed a clear staining of the hippocampus, in CA1 and DG cell layers (Fig. 1D). In *Pak3*-R67C mice, basal neuronal architecture of the hippocampal anatomy appeared normal (Fig. 1E). The volume of the dorsal hippocampus was comparable in WT and *Pak3*-R67C mice (Mann–Whitney test: dorsal hippocampus, p=0.91).

General behavior of *Pak3*-R67C mice

Male *Pak3*-R67C mice appeared healthy and showed no overtly abnormal behavior. In the open-field, both genotypes (12 WT and 15 *Pak3*-R67C mice) showed a progressive and significant reduction of the distance traveled over a 40-min testing period (Supplementary Fig. 1A; repeated measures ANOVA time effect: $F(7,175)=26.79$, $p<0.001$; genotype effect: $F(1,25)=0.09$, $p=0.76$; interaction: $F(7,175)=0.41$, $p=0.89$), with no genotype difference in running speed ($F(1,25)=0.09$, $p=0.76$), maximal speed ($F(1,25)=0.11$, $p=0.73$) and vertical activity (Supplementary Fig. 1B; $F(1,25)=0.22$, $p=0.64$), suggesting absence of major motor deficits or hyperactivity during exploration of a novel environment. Behavioral activity displayed in the center area of the open-field, which may typically reflect anxiety-related responses, was also unaltered in *Pak3*-R67C mice, as reflected by a lack of genotype difference in the latency to enter in this area ($F(1,25)=0.58$, $p=0.45$), in the number of entries ($F(1,25)=0.11$, $p=0.73$), the percent time spent (Supplementary Fig. 1C; $F(1,25)=1.83$, $p=0.18$) and the distance traveled in the center area ($F(1,25)=1$, $p=0.32$).

Impaired long-term spatial memory in *Pak3*-R67C mice in massed but not in distributed training protocols

We analyzed spatial learning and memory performance in the water maze using two distinct training protocols with two different cohorts of mice. When training was distributed over 11 days (4 successive trials per day), mice of both genotypes showed comparable learning curves (Fig. 2A, 12 WT and 15 *Pak3*-R67C mice), as reflected by the decrease in escape latency (repeated measures ANOVA, days: $F(10,250)=19.099$, $p<0.0001$; genotype: $F(1,25)=0.093$, $p=0.7634$; interaction: $F(10,250)=0.395$, $p=0.9482$) and in the distance swum to find the platform (repeated measures ANOVA, days: $F(10,250)=13.243$, $p<0.0001$; genotype: $F(1,25)=2.161$, $p=0.154$; interaction: $F(10,250)=0.456$, $p=0.9167$). The swim speed was globally higher in *Pak3*-R67C mice (Supplementary Fig. 2A, genotype: $F(1,25)=9.002$, $p=0.006$; interaction: $F(10,250)=0.614$, $p=0.8018$). However, the genotype difference in swim speed was not significant during the first two days (genotype: $F(1,25)=2.356$, $p=0.1374$), suggesting it was induced by the learning procedure rather than reflecting changes in the initial motor performance. Thigmotaxis decreased significantly over training in both genotypes (Supplementary Fig. 2B, days: genotype: $F(1,25)=0.257$, $p=0.6168$; days: $F(10,250)=21.763$, $p<0.0001$; interaction: $F(10,250)=1.629$, $p=0.0987$). During the probe test performed 48h after the last training session (Fig. 2B), mice of both genotypes showed a preference for the target quadrant and the percent time spent in this target quadrant was significantly different from the 25% chance level in both genotypes (Fig. 2B; factorial ANOVA, genotype: $F(1,25)=0.298$, $p=0.5902$; one sample *t* test, WT: $t(11)=2.705$, $p=0.0205$; *Pak3*-R67C: $t(14)=3.395$, $p=0.0044$). Although the swim speed was higher in *Pak3*-R67C than in WT mice during this trial ($F(1,25)=10.04$, $p=0.004$), both genotypes displayed comparable number of crossings ($F(1,25)=0.37$, $p=0.54$) and percent distance swum in the target quadrant ($F(1,25)=0.822$, $p=0.3731$). In a second probe test performed one week post-training (Fig. 2C), mice of both genotypes displayed comparable performance and the percent time spent in the target quadrant during this trial was significantly different from chance level (Fig. 2C; factorial ANOVA, genotype: $F(1,25)=0.105$, $p=0.7484$; one sample *t* test, WT: $t(11)=2.204$, $p=0.0497$; *Pak3*-R67C: $t(14)=5.868$, $p<0.0001$). They also showed comparable number of crossings ($F(1,25)=0.006$, $p=0.93$) and percent distance swum ($F(1,25)=0.001$, $p=0.97$).

We then submitted another cohort of WT (n=7) and *Pak3*-R67C (n=6) mice to a more stringent spatial learning and memory task using a massed training protocol performed within a single day in the water

maze, an experimental design that is more sensitive than distributed training in certain genetically-modified mice (26) or in mice with altered hippocampal neurogenesis (27, 28) and analyzed long-term spatial memory performance 10 days after training. During training, the swim path lengths and time to reach the platform decreased significantly in both genotypes (Fig. 2D; repeated measures ANOVA, distance: genotype: $F(1,11)=0.002$, $p=0.9623$; trials: $F(8,88)=7.686$, $p<0.0001$; interaction: $F(8,88)=0.918$, $p=0.5061$; time to find the platform: genotype: $F(1,11)=0.126$, $p=0.7298$; trials: $F(8,88)=4.567$, $p=0.0001$; interaction: $F(8,88)=0.884$, $p=0.5334$), as observed in the distributed protocol. Swim speed and thigmotaxis were also similar between genotypes (Supplementary Fig. 2C and 2D, repeated measures ANOVA, swim speed: genotype: $F(1,11)=0.407$, $p=0.5368$; trials: $F(8,88)=4.236$, $p=0.0002$; interaction: $F(8,88)=0.447$, $p=0.8894$; thigmotaxis: genotype: $F(1,11)=0.193$, $p=0.6691$; trials: $F(8,88)=27.450$, $p<0.0001$; interaction: $F(8,88)=0.572$, $p=0.7985$). Hence, mice from both genotypes learned similarly the task. Spatial long-term memory was probed 10 days later. In contrast to WT mice who spent significantly more time in the target quadrant, *Pak3*-R67C mice spent as much time in the target quadrant as in the other quadrants (Fig. 2E; repeated measures ANOVA, genotype: $F(1,11)=7{,}241$, $p=0.0210$; quadrant: $F(1,11)=11.387$, $p=0.0062$; interaction: $F(1,11)=7{,}425$, $p=0.0198$; one sample *t* test, target quadrant: WT $t(6)=4.708$, $p=0.0033$; *Pak3*-R67C $t(5)= 0.418$, $p=0.6934$). The mean number of crossings of the platform location was significantly smaller in *Pak3*-R67C than in WT mice (Fig. 2F; factorial ANOVA, $F(1,11)=5.242$, $p=0.0428$) and *Pak3*-R67C displayed slightly longer distance swum before reaching the target platform position (factorial ANOVA, distance before first crossing: $F(1,11)=5.461$, $p=0.0394$). During this probe test, swim speeds were comparable between genotypes (factorial ANOVA, $F(1,11)=2.674$, $p=0.1302$). Hence, despite normal spatial learning in both protocols, *Pak3*-R67C mice displayed long-term spatial memory deficits in the more difficult massed training protocol.

Normal spatial working memory but spatial pattern separation deficit in *Pak3*-R67C mice

We then examined mice performance in a radial-maze to evaluate their working memory and their ability to finely discriminate spatial configurations. In the working memory paradigm, in which mice had to recover rewards located at the end of the 8 arms of the radial maze without returning to a

previously visited arm, both genotypes showed an identical progressive increase of the number of correct trials (10 WT and 11 *Pak3*-R67C mice; Supplementary Fig. 1D, repeated measures ANOVA, genotype: $F(1,16)=1.444$, $p=0.2470$; days: $F(10,160)=4.750$, $p<0.0001$; interaction: $F(10,160)=0.738$, $p=0.6878$) suggesting that *Pak3*-R67C mice do not display working memory deficits in this task.

Then, to analyze spatial pattern separation function, we submitted *Pak3*-R67C and WT mice to a spatial delayed non-matching to place (DNMP) paradigm in the radial-maze (29, Fig.3A). During this task (4 trials/day during 10 days), mice (18 WT and 17 *Pak3*-R67C mice) were tested for their ability to distinguish two spatial configurations that differed by a variable distance between two arms positions of the radial-arm maze. In each trial, mice were submitted to a sample phase in which they can run from a start arm to a single open rewarded arm of the maze and, after a 20s delay, were replaced into the start arm and had to choose between the previously rewarded arm (now non-baited) and a new open and rewarded arm. This newly rewarded arm could be either close or distant to the previously visited arm (Fig. 3A) and the sets of 3 arms varied randomly among trials and during the 10 days of the experiment. Thus, this paradigm tests the ability to spatially discriminate between 2 arms of the maze, either spatially close to each other ("close" configuration) or more separated ("distant" configuration; see methods). In both genotypes, the percent of correct trials in both "close" and "distant" configurations increased regularly over the 10 days of training (Fig. 3B). In the distant configuration, this improvement of performance reached statistical significance in both genotypes (repeated measures ANOVA, "distant" WT: $F(4,68)=4.010$, $p=0.0056$; *Pak3*-R67C: $F(4,64)=4.510$, $p=0.0028$). However, in the close configuration, there was a trend towards significance in WT mice, but not in *Pak3*-R67C mice (repeated measures ANOVA, "close" WT: $F(4,68)=2.201$, $p=0.0780$; *Pak3*-R67C: $F(4,64)=1.785$, $p=0.1427$). In both cases, the genotype effect and the percent correct trial x genotype interaction were non-significant ("close": $F(1,33)=0.077$, $p=0.7829$ and $F(4,132)=1.650$, $p=0.1654$; "distant": $F(1,33)=2.382$, $p=0.1323$ and $F(4,132)=1.168$, $p=0.3277$, respectively). By the end of training (D9-10), however, performance in both configurations and for both genotypes differed significantly from chance (Fig. 3B; one sample *t* test, D9-10: "close": WT: $t(17)=3.828$, $p=0.0013$; *Pak3*-R67C: $t(16)=2.393$, $p=0.0293$; "distant": WT: $t(17)=5.236$, $p<0.0001$; *Pak3*-R67C: $t(16)=3.887$,

p=0.0013). These results suggest no specific deficit in *Pak3*-R67C mice during the training phase of this task, whatever the configuration (close or distant). On day 11, we separated the initial group into two sub-groups of each genotype, which were each submitted to a probe test with 3 successive trials in only one given configuration (either in the close configuration: 9 WT and 9 *Pak3*-R67C mice or the distant configuration: 9 WT and 8 *Pak3*-R67C mice). During this probe test, WT mice performed well in both configurations (Fig. 3C; one-sample analysis to chance: close configuration t(8)=4.359, p=0.0024, distant configuration t(8)=2.887, p=0.0203), while, in contrast, *Pak3*-R67C mice remained at chance level in the close configuration despite their good performance in the distant configuration (Fig. 3C; percent correct trials: "close": Factorial ANOVA: F(1,16)=7.143, p=0.0167; one sample *t* test to chance: *Pak3*-R67C t(8)=-0.164, p=0.8735; "distant": Factorial ANOVA: F(1,15)=0.176, p=0.6804; one sample *t* test to chance: *Pak3*-R67C t(7)=3.742, p=0.0072). This suggests a hippocampal-dependent spatial pattern separation deficit in *Pak3*-R67C mice in conditions of higher interference due to the immediate succession of 3 consecutives trials with the same configuration.

Hippocampal pattern separation deficit and high sensitivity to interference in irradiated WT mice and in *Pak3*-R67C mice

The pattern of deficits observed in *Pak3*-R67C mice, selectively expressed as a long-term spatial memory deficit when retention was tested several days after massed training and as a spatial pattern separation deficit under high interference, is a common phenotype observed in mice with altered adult hippocampal neurogenesis (7, 27, 28, 29). Moreover, there are hints to suggest that altered hippocampal neurogenesis can affect the proper management of interference (30, 31, 32). To test this hypothesis more specifically, we used another cohort of mice to examine their performance in a hippocampal-dependent successive spatial delayed non-matching to place task developed by Al Abed et al. (33), which tests memory flexibility and the ability to overcome proactive interference. This task in a radial-maze requires the ability to retain recently visited places, i.e. to remember which arm was the more recently visited arm within each of 3 repeatedly used pairs of arms, over varying intervals (Fig. 4A-B). This task is therefore characterized by high organizational demand due to the varying delay separating repetitions of similar events (33, and see methods). During behavioral testing, each

mouse was attributed a set of 3 pairs of adjacent arms presented in a pseudo-random order (Fig. 4A). For each arm pair, the position of the reward was alternated between one trial of that pair and the next one of the same pair (Fig. 4B). During the 15 days of training, mice were submitted to 23 successive trials with a 10 s inter-trial interval (ITI). Performance was measured as the percentage of correct trials over training and, for the last 3 days of training, proactive interference (PI) was calculated as a function of the number of interfering trials (ITn) that corresponds to the number of trials between 2 trials of the same pair (see methods for details). Using c-Fos labeling, Al Abed et al. (33) showed that realization of the task relies heavily on DG activity and pattern separation function. Although this is suggestive of a possible involvement of DG newborn neurons, there is as yet no evidence that adult neurogenesis blockade would cause deficits in this task. To investigate this point, we first tested in this behavioral task performance of WT mice submitted to targeted irradiation of the dorsal DG to focally ablate their adult born neurons (34). For this, a group of 10 C57BL/6 wild-type mice were exposed to X-ray ionizing radiation using the Small Animal Radiation Research Platform (SARRP) of IRSN (Fontenay-aux-Roses, France, see methods), which delivers targeted radiation to the dorsal DG with high accuracy, following the methods and protocol described in (34). Eight non-irradiated sham mice (NIR) served as controls (see methods). To avoid potential advert effects of neuroinflammation caused by irradiation, mice were trained two months after irradiation (29, 35). Using the BrdU marker, we confirmed the near complete blockade of dorsal DG neurogenesis in irradiated (IR) mice compared to NIR mice (Supplementary Fig. 3 A; Mann–Whitney test: $p=0.0090$). An additional count of DCX^+ cells in the dorsal and the ventral DG showed a significant decrease in the number of immature adult-born neurons in the dorsal DG of IR mice, while the densities of DCX^+ cells were comparable in both groups of mice in the ventral DG (Supplementary Fig. 3 B-D; Mann–Whitney test, dorsal DG: $p=0.0209$; ventral DG: $p=0.0833$), thus confirming the specific irradiation of dorsal DG. In the behavioral task, the percentage of correct choices increased significantly during training in non-irradiated (NIR) mice, whereas performance of irradiated (IR) mice remained at chance level (Fig. 4C; percent correct choices: IR/NIR group effect: $F(1,16)=7.815$, $p=0.0130$; time: $F(4,64)=13.748$, $p<0.0001$; interaction: $F(4,64)=4.703$, $p=0.0022$). During the final block of 3 days (block 5, Fig.4C), the percent of correct choices of NIR mice was significantly higher than that of IR mice (Factorial

ANOVA: group: F(1,16)=18.816, p=0.0005). Performance was then expressed as a function of the number of interfering trials (ITn) between two presentations of the same pair. This revealed that performance of NIR mice became slightly lower (from 80% to 72% correct) as the ITn increased, but remained significantly above chance whatever the ITn (Fig. 4D; one sample *t* test ITn 0: NIR: t(7)=9.756, p<0.0001; ITn 1-2: NIR: t(7)=9.888, p<0.0001; ITn 3-4: NIR: t(7)=5.173, p=0.0013). In contrast, performance of IR mice decreased when the ITn increased and was significantly different from NIR mice both for an ITn 1-2 and an ITn 3-4 (Fig. 4D; Factorial ANOVA: ITn 0: F(1,16)=2.264, p=0.1519; ITn 1-2: F(1,16)=7.979, p=0.0122; ITn 3-4: F(1,16)=11.228, p=0.0041), yet it remained above chance level whatever the ITn (Fig. 4D; one sample *t* test: IR: ITn 0: t(9)=6.845, p<0.0001; ITn 1-2: t(9)=2.490, p=0.0344; ITn 3-4: t(9)=2.262, p=0.05). Finally, analysis of proactive interference (PI) analyzed in the final block of 3 days (block 5; Fig. 4E) revealed that unlike NIR mice, IR mice displayed a strong negative proactive interference effect in both the low and high PI conditions (Fig. 4E; Factorial ANOVA: low PI, F(1,16)=8.459, p=0.0103; one sample *t* test NIR: t(7)=8.412, p<0.0001; IR: t(9)=1.112, p=0.2948; high PI, F(1,16)=5.659, p=0.0302; one sample *t* test NIR: t(7)=3.906, p=0.0059; IR: t(9)=2.255, p=0.0506). Altogether, these results suggest that adult-born neurons in the dorsal DG play an important role in the ability to organize events in memory as they are used and to overcome interference.

We then tested performance of a cohort of WT (n=13) and *Pak3*-R67C (n=13) mice in this task. During training, the percentage of correct choices increased significantly in WT mice, whereas performance of *Pak3*-R67C mice remained at chance level (Fig.4F; percent correct choices: genotype: F(1,24)=11.974, p=0.0020; time: F(4,96)=16.388, p<0.0001; interaction time x genotype F(4,96)=3.551, p=0.0095). At the end of training (block 5), WT mice displayed significantly more correct choices than *Pak3*-R67C mice (Fig. 4F, Factorial ANOVA: genotype: F(1,24)=15.662, p=0.0006). Performance in the final block of 3 days (block 5-Fig. 4G) was also expressed as a function of the ITn between two presentations of the same pair. This analysis showed that performance of WT mice decreased slightly (from 87% to 65% correct) as the ITn increased, but remained significantly above chance level even for the ITn 3-4 (Fig. 4G). In contrast, performance of *Pak3*-R67C was significantly lower compared with WT mice, whatever the number of interfering trials, even when

there was no interfering trial (ITn 0). Moreover, their percent of correct choices was at chance level for the ITn 3-4 (Fig. 4G; Factorial ANOVA: genotype: ITn 0: $F(1,24)=5.577$, $p=0.0267$; one sample *t* test WT: $t(12)=11.677$, $p<0.0001$; *Pak3*-R67C: $t(12)=7.580$, $p<0.0001$; ITn 1-2: $F(1,24)=11.234$, $p=0.0027$; one sample *t* test WT: $t(12)=8.768$, $p<0.0001$; *Pak3*-R67C: $t(12)=2.683$, $p=0.0199$; ITn 3-4: $F(1,24)=13.047$, $p=0.0014$; one sample *t* test WT: $t(12)=4.754$, $p=0.0005$; *Pak3*-R67C: $t(12)=0.770$, $p=0.4563$). Finally, analysis of proactive interference (PI) in the final block of 3 days (block 5; Fig. 4H) revealed that unlike WT mice, *Pak3*-R67C mice displayed a strong negative proactive interference effect at high but not low PI (Low PI: Factorial ANOVA: $F(1,24)=2.949$, $p=0.0988$; one sample *t* test WT: $t(12)=6.470$, $p<0.0001$; *Pak3*-R67C: $t(12)=3.448$, $p=0.0048$; High PI: Factorial ANOVA: $F(1,24)=5.023$, $p=0.0345$; one sample *t* test WT: $t(12)=4.415$, $p=0.0008$; *Pak3*-R67C: $t(12)=1.516$, $p=0.1554$). The deficits observed in *Pak3*-R67C mice in this task indicate that they exhibited a higher sensitivity to high proactive interference. Altogether, the deficits observed in irradiated mice suggest that adult-born neurons in the dorsal DG play an important role in the ability to organize events in memory as they are used and to overcome interference. Likewise, these functions are affected in mice carrying the R67C mutation of the *Pak3* gene, suggesting, together with the observed deficits in spatial long-term memory and in spatial pattern separation function, that PAK3 dysfunction could be associated with altered adult hippocampal neurogenesis.

Selective alterations of adult DG neurogenesis in *Pak3*-R67C mice

As previously shown, PAK3 is expressed in the DG (Fig. 1D). To specify the identity of the cells expressing PAK3 in DG, we performed immunofluorescence labeling on lacZ-stained sections of *Pak3*-tm1b-lacZ reporter mice with neuronal markers. As shown in Fig.5A, most PAK3 expressing cells were localized in the subgranular zone of the DG. They expressed NeuN and some of them co-expressed DCX, suggesting that PAK3 is expressed in both mature and immature neurons of the DG. The volume of the DG and of the granule cell layer (GCL) were both comparable in WT and *Pak3*-R67C mice (Mann–Whitney test: DG, $p=0.91$; GCL; $p=0.6$). The mean number of mature neurons ($NeuN^+$ cells) in selected zones of the DG was also comparable (WT: 1445 ± 98.718 $NeuN^+$ cells; *Pak3*-R67C: 1357 ± 59.943 $NeuN^+$ cells; Mann-Whitney test: $p=0.7728$). We then examined

proliferation, differentiation and survival of adult-generated cells in the DG of *Pak3*-R67C mice and WT littermates in basal conditions. Using the proliferation marker Ki67, we found similar densities of $Ki67^+$ cells in both genotypes (Fig. 5B; Mann–Whitney test: $p>0.9999$), suggesting that proliferation of newborn cells in adult DG was not affected by the R67C mutation of *Pak3*. Newborn cell survival was studied at different times after BrdU injections (18, 28 and 38 days post injections, dpi; Fig. 5C). As expected, a high rate of newborn cells was eliminated in both WT and *Pak3*-R67C mice within the first few weeks after their birth. However, while WT mice showed a progressive loss of $BrdU^+$ cells between 18 and 38 dpi, an accelerated death was observed in *Pak3*-R67C mice with a salient loss between 18 and 28 dpi (Mann–Whitney test: 18 dpi: $p=0.6242$; 28 dpi: $p=0.0275$; 38 dpi: $p=0.4624$). This accelerated death did not, however, affect the whole population of newborn neurons, since the number of surviving dentate granule cells (DGC) appeared equivalent to that of WT mice several weeks later (38 dpi) (Fig. 5C). We also verified whether this accelerated death had any consequences for the population of immature DCX^+ neurons. Comparable densities of immature DCX^+ neurons were observed in the DG of WT and *Pak3*-R67C mice (Fig. 5D; Mann–Whitney test: $p=0.1416$). Likewise, triple labeling of $BrdU^+$ cells with markers of immature (DCX) and mature (NeuN) neurons at different dpi revealed no significant differences between genotypes (Fig. 5E-F; Mann–Whitney test: 18 dpi: $BrdU^+/DCX^+/NeuN^+$ cells: $p=0.2159$; $BrdU^+/DCX^-/NeuN^+$ cells: $p>0.9999$; 28 dpi: $BrdU^+/DCX^+/NeuN^+$ cells: $p=0.5637$; $BrdU^+/DCX^-/NeuN^+$ cells: $p=0.4705$; 38 dpi: $BrdU^+/DCX^-/NeuN^+$ cells: $p=0.0864$). Moreover, double labeling of 18-day-old $BrdU^+$ cells with the glial maker Glial fibrillary acidic protein (GFAP) also revealed no difference between genotypes (data not shown; Mann–Whitney test: 18 dpi: $BrdU^+/GFAP^+$ cells: $p=0.4705$). Overall, these results indicate normal proliferation, fate determination, differentiation rate and neuronal phenotypic maturation over time among the surviving neurons in *Pak3*-R67C mice. However, the R67C mutation of the *Pak3* gene was associated with a selective, albeit transient, deficit in the survival of a population of adult-born DGC within the critical time-window during which they are usually selected to die or survive for long-term functional integration into pre-existing cortico-hippocampal networks.

Delayed functional and morphological maturation and deficient recruitment of newborn DGCs into spatial memory networks

Guided by the evidence that adult-born DGCs can be recruited upon hippocampal-dependent spatial learning (7, 28, 36, 37, 38), we studied the activation of adult-born DGC following spatial memory recall using the activation marker Zif268. For this, we used mice trained in the massed training regimen in the water maze described above, since *Pak3*-R67C mice can learn this task as well as WT mice, but show severe memory deficits 10 days post-training (Fig. 2E-F). *Pak3*-R67C and WT mice were submitted to the task 18 days after BrdU injections and newborn cells survival and Zif268 expression were analyzed after the probe test 10 days after the end of the training (Fig. 6A). Counting $BrdU^+$ cells after the retention test showed that our training conditions did not impact survival of newborn DGCs aged 18 days at the time of learning, neither in WT nor in *Pak3*-R67C mice as compared to home cage controls (HC-CTRL, Fig. 6B; Mann–Whitney test: WT: $p>0.9168$; *Pak3*-R67C: $p>0.9999$). The number of 28-day-old newborn DGCs was significantly lower in *Pak3*-R67C mice than in WT mice (Fig. 6B; Mann–Whitney test: $p=0.0275$), similarly to what was observed in home cage controls (Fig. 5C at 28dpi and 6B HC-CTRL). We then examined whether the R67C mutation affects the activity-dependent recruitment of DG neurons by mapping Zif268 expression in newborn immature neurons (DCX^+), in 28-day-old neurons ($BrdU^+/NeuN^+$) and in "older" mature neurons ($NeuN^+$) after memory recall. In control home cage WT and *Pak3*-R67C mice, there was virtually no activation of immature DCX^+ neurons and only a small proportion of 28-day-old DGCs ($BrdU^+/NeuN^+/Zif268^+$) and mature neurons ($Zif268^+/NeuN^+$) expressed Zif268, with no significant difference between genotypes (Fig. 6C-E; Mann–Whitney test: $BrdU^+/NeuN^+/Zif268^+$: $p=0.5637$; $Zif268^+/NeuN^+$: $p=0.3865$). After memory recall, a significant proportion of younger, DCX^+ newborn DGCs expressed Zif268 in WT mice compared to HC CTRL (Fig. 6C; Mann–Whitney test: WT: $p=0.0209$), suggesting recruitment of a small proportion of these immature neurons as previously published (28, 37, 39). In contrast, no neurons within this population were activated upon recall in *Pak3*-R67C mice (Fig. 6C). For 28-day-old $BrdU^+$ neurons, the proportion of cells expressing Zif268 was similar between genotypes and not different from controls (Fig. 6D; Mann–Whitney test: WT: $p=0.6242$; *Pak3*-R67C: $p=0.7728$), suggesting this population of neurons was not specifically

activated upon recall and not impacted by the dysfunction of PAK3. Finally, the proportion of mature neurons expressing Zif268 in WT mice after memory recall was significantly higher than in the HC condition (Fig. 6E; Mann–Whitney test: WT: p=0.05). Although this increase after recall did not reach significance in *Pak3*-R67C mice (Fig. 6E; Mann–Whitney test: *Pak3*-R67C: p=0.2207), there was no significant genotype difference in the proportion of $Zif268^+/NeuN^+$ cells after recall (Fig. 6E; Mann–Whitney test: p=0.6015). Thus, memory recall in our training conditions resulted in an activation of a similar proportion of mature DGCs in WT and *Pak3*-R67C mice, and a selective, learning-related activation of a population of young immature neurons in WT mice, which failed to be activated in *Pak3*-R67C mice. This suggests that the long-term spatial memory deficit in *Pak3*-R67C mice is associated with the absence of recruitment of this neuronal population by learning.

This specific phenotype of *Pak3*-R67C mice has also been observed in another mutant mouse for which deletion of the gene *Zif268* led to a similar accelerated death during the critical window of maturation of newborn DGCs and a defect of recruitment during learning, effects that were attributed to delayed functional maturation and altered morphological maturation of young newborn DGCs (28). Indeed, around 3 weeks of age, newborn DGCs undergo extensive functional synaptic changes that are essential for their functional maturation and their survival (40). At this age, the cells start to express the AMPA-type glutamate receptor GluA1 (41) and also the Cl^- ionic co-transporter, KCC2b, that contributes to the formation of mature dendritic spines and functional excitatory synapses (42) and is implicated in the conversion from GABA-induced depolarization to hyperpolarization, a mechanism crucial for synaptic integration of 3-week-old DGCs (43, 44). We therefore analyzed GluA1 and KCC2b expression in 18-day-old DGCs of *Pak3*-R67C and WT mice. We found that the proportion of BrdU-labeled 18-day-old newborn DGCs expressing GluA1 was similar between genotypes (data not shown; Mann-Whitney test: p>0.9999). However, the expression pattern of KCC2b revealed a significant decrease in the expression of this Cl^- co-transporter in BrdU-labeled 18-day-old DGCs of *Pak3*-R67C mice compared to WT mice (Fig. 7A-B; Mann-Whitney test: KCC2b: p=0.0090). We also analyzed the dendritic morphology of immature neurons (DCX^+ cells; Fig. 7 C-E). We found that the total length of dendrites of DCX^+ cells was significantly shorter in *Pak3*-R67C compared to WT mice (Fig. 7D, Mann–Whitney test: p=0.009), with significantly less dendritic branching (Fig. 7E, Mann–

Whitney test: p=0.009). Thus, given the role of KCC2b in neuronal maturation and in the conversion of GABA-mediated depolarization to hyperpolarization, our result could indicate in *Pak3*-R67C mice, a delayed functional maturation of young newborn DGCs during their critical window of maturation and selection, associated with impairment in their morphological development. These effects might be instrumental in their accelerated death during this time period and lack of recruitment in relation to learning and memory.

Discussion

In the present work, we generated a novel mouse model of ID bearing the missense mutation R67C of the *Pak3* gene to characterize the effect of this mutation in cognitive functions and explore the possibility that the cognitive deficits caused by this mutation may be associated with altered adult hippocampal neurogenesis. The mutation generated in our mouse model is strictly similar to the human mutation (22). The knock-in mutation did not alter the expression of the mutated gene suggesting that the mouse phenotype is not due to a defect of *Pak3* gene expression or PAK3 protein synthesis. Hemizygous males and heterozygous females displayed normal life and were fertile. Moreover, the R67C mutation did not alter the volume and general organization of the hippocampal formation, in line with the absence of major brain morphological defect reported in patients bearing this mutation in a three-generation tree (21, 22).

Our behavioral characterization showed that *Pak3*-R67C mice display normal locomotion and exploration, no specific alteration of anxiety-like behaviors and no deficit in spatial working memory in a radial maze. We also report that *Pak3*-R67C mice do not display spatial learning and memory deficits in a distributed protocol in the water-maze. However, using a more stringent spatial learning task based on a massed protocol, we found that despite normal spatial learning, long-term spatial memory was deficient in *Pak3*-R67C mice. Moreover, using a delayed non-matching to place task placing varying demands on spatial discrimination ability (29), we showed that *Pak3*-R67C mice display alterations in spatial pattern separation function and a higher sensitivity to interferences. This

was confirmed in the hippocampal-dependent successive spatial delayed non-matching to place task that models declarative memory of repetitive everyday events (33). This task in a radial-maze is characterized by high organizational demand due to the varying delay separating repetitions of similar events and allows probing memory flexibility and organization, and susceptibility to proactive interference. Our results show that, despite normal spatial working memory, *Pak3*-R67C mice exhibit a higher sensitivity to proactive interference, suggesting impaired organization of events in memory. Together, these results demonstrate for the first time a link between PAK3 dysfunction and alterations in spatial memory, in pattern separation function and notably in the management of interference, which are in line with impaired spatial cognitive skills and deficits in attentional and executive functions reported in patients holding mutations in the *Pak3* gene (45).

Numerous studies showed that defects in adult hippocampal neurogenesis result in alterations of spatial memory and pattern separation function (29, 46, 47). Reports also suggest the involvement of dentate gyrus adult-born neurons in behavioral tasks involving proper management of interferences (30, 48, 49). Here, we first strengthen this point in the successive spatial delayed non-matching to place task by examining performance of normal mice subjected to targeted X-ray irradiation of the dorsal dentate gyrus. Our results showed that mice with near complete absence of adult-born neurons in the dorsal hippocampus have profound deficits in the task characterized by a higher sensitivity to proactive interference. Although our experiment does not address the potential differential contribution of hippocampal adult born neurons in the dorsal and ventral parts of the DG in this task, the similarities between the behavioral phenotype of *Pak3*-R67C mice and that found after irradiation of the dorsal DG in WT mice reinforce our hypothesis that adult hippocampal neurogenesis might be one neurobiological mechanism altered in our transgenic mice.

PAK3 is expressed in hippocampus (24) and we confirmed here, by a genetic approach, its expression in granule cells of the adult DG, including in immature DCX-expressing neurons. Our analyses showed that, in basal conditions, the R67C mutation of *Pak3* does not affect cell proliferation and neuronal differentiation of adult-born DGCs. In contrast, young immature newborn neurons in *Pak3*-R67C mice undergo accelerated death during the critical period, around 3-4 weeks of their birth,

which we associated with a potential deficient functional maturation, as indicated by the low percentage of young newborn neurons expressing the KCC2b chloride co-transporter and the reduced or delayed morphological development of their dendritic arborisations. Despite the fact that the number of surviving DGCs 38d after their birth appeared equivalent to that of WT mice, this accelerated death of newborn neurons and their altered functional maturation during the critical period could be one potential mechanism leading to cognitive deficits. Indeed, young adult neurons, even still immature, play an important role in hippocampal-dependent forms of memory (reviewed in 50, 51, 52). To date, several extrinsic and intrinsic cell-signaling factors can regulate adult neurogenesis during their critical period of maturation (≈2-6 weeks after their birth) and influence the destiny of newborn cells, promoting either their death (for the majority) or their survival and integration into pre-existing cortico-hippocampal networks (for reviews, 50, 40). The general scenario suggests that when a specific hippocampal-dependent learning experience occurs, a number of young newborn DGCs, because of their high intrinsic excitability and high capacity to undergo synaptic potentiation (43), are activated by learning, promoting their recruitment and functional integration into memory networks, and hence their subsequent activation upon memory recall (39). We thus investigated the recruitment of DG neurons by measuring Zif268 expression after recall of spatial learning in the massed paradigm for which *Pak3*-R67C mice display normal learning but deficient long-term memory. We found memory recall resulted in normal activation of mature DG and 28-day-old $BrdU^+$ neurons in *Pak3*-R67C mice, but there was a complete failure of recruitment of a population of young DCX^+ newborn neurons, indicating that the long-term spatial memory deficit in these mice is associated with the absence of recruitment of this population of young newborn neurons. We therefore propose that the R67C mutation of *Pak3* leads to a specific, transient loss of young, not fully mature DGCs during their critical period of maturation. This in turn would impede the recruitment of a population of these young newborn neurons by training, preventing their contribution to long-term spatial memory. Whether this alteration in adult neurogenesis and deficient activation upon learning is also causative for the altered capacity of the mutant mice to cope with interferences and for their deficient ability to finely discriminate events in the spatial domain remains to be investigated. Although there are many unknowns about brain alterations associated with the R67C mutation of the *Pak3* gene, the

documented contribution of adult hippocampal neurogenesis to spatial memory and spatial pattern separation function (7, 27, 28, 29, 46, 47, 53) reinforces the hypothesis that altered adult neurogenesis in *Pak3*-R67C mice might be one mechanism instrumental in the selective behavioral deficits displayed by the mice.

Mechanistically, how the R67C mutation of the *Pak3* gene could lead to an altered adult hippocampal neurogenesis is as yet unknown. The R67C mutation is located in the regulatory domain of the protein, which changes PAK3 binding to the Rho-GTPase Cdc42 and Rac1, impairing PAK3 binding to Cdc42 while increasing binding to Rac1 (23). Interestingly, it was reported that Cdc42 and Rac1 are differentially regulated during adult hippocampal neurogenesis, suggesting they have stage-specific functions (54). Briefly, Cdc42 plays an important role in the proliferation of neural stem/progenitor cells, is enriched in DCX^+ immature neurons and its activity is associated with initial dendritic development and dendritic spine maturation. Rac1, in contrast, is mainly operational and crucial in late stages of dendritic outgrowth and spine maturation. Here, we found that the dysfunction of PAK3 does not affect the proliferation of adult born cells, suggesting that Cdc42-PAK3 binding is not required in this step during adult hippocampal neurogenesis. Concerning neuronal maturation, it has previously been shown in cultured hippocampal neurons that the R67C mutation affects spine density, suggesting altered spine growth, from initiation to stabilization of newly formed spines (23). Thus, because dendritic maturation of young adult-born neurons appeared altered by the R67C mutation, the recruitment failure of young DCX newborn neurons when learning occurs is likely due to a defect or a delay in spinogenesis of these young neurons, perhaps because Cdc42-PAK3 binding is reduced when PAK3 holds the R67C mutation. Future work will be necessary to confirm whether the R67C mutation of *Pak3* alters the formation of dendritic spines of young adult hippocampal neurons *in vivo*, and what are the underlying molecular mechanisms. Finally, although we found that young DCX^+ neurons can express PAK3, we cannot discard a cell non-autonomous function of PAK3. Cell type-specific manipulation of mutated PAK3 using genetic approaches will be one step further for dissociating cell-autonomous and non cell-autonomous contribution of PAK3.

In summary, this study allowed us to find that the R67C mutation of the *Pak3* gene in mice recapitulates some of the human ID phenotypes, especially in the spatial memory domain when the tasks require rapid learning and place a high demand on spatial discriminability and the management of interferences. We also highlighted that the R67C mutation causes dysfunctional maturation and learning-associated recruitment of a population of young adult-born hippocampal neurons during their critical period of integration into pre-existing cortico-hippocampal networks, a defect that represents one possible mechanism contributing to the observed cognitive impairments.

Materials and Methods

Generation of *Pak3*-R67C knock-in mice

The 8.6 kb genomic fragment corresponding to the 143.704.924 to 143.713.589 nucleotides from the mouse X chromosome in the genome assembly reference sequence GRCm38.p4 containing the coding exon 2 of the C57Bl/6N mouse *Pak3* gene was subcloned from a BAC plasmid into the backbone vector pHL931. The modified arm containing the coding exon 2 of *Pak3* (0.8 kb) and the floxed neomycin selection cassette were inserted between the 5' homology arm (4.5 kb) and the 3' arm (3.5 kb) by PCR. Directed mutagenesis of the g>143709671 C>T was done by PCR and DpnI digestion and verified by sequencing. The linearized vector was electroporated into the ES cell line MCI-C57BL/6N. 361 neomycin-resistant clones were screened for homologous recombination by PCR and 5 positive clones were further confirmed by Southern blotting after DNA genomic digestion with AseI and NdeI to validate the 5' arm insertion, and SexAI and XcmI to validate the 3' arm insertion. Two selected clones were injected in blastocysts and embryo transfer to pseudo-pregnant females was performed by standard procedures. Offspring (F1) with the coat color characteristic for the ES background were tested for germ line transmission by PCR and further confirmed by Southern blot analysis. In order to remove the positive selection marker, 8-week old positive F1 mice were then bred with recombinase-expressing C57BL/6 mice (55). Segregation of the targeted gene and Cre-recombinase alleles were also monitored by Southern blot analysis. As the missense mutation

suppresses a restriction enzyme H*haI* site (22), the corresponding genomic region of a *Pak3*-R67C male was PCR-amplified from genomic DNA with high-fidelity Taq polymerase and the two primers 5'-GCTTTCTTATGCAGTGTATGCAAGCCA and 5'-GGAGGAAAAGTTTCCATCTTCAGACTGAC, and the amplified PCR fragment was H*haI* digested and fragments analyzed by electrophoresis on agarose gels. PCR fragments were also cloned and several clones were sequenced. The genotype of mutated mice was routinely determined by PCR analysis using primers encompassing the lox sequences (forward primer 5-GTGGGTTTTGATGCAGTCACCGG and reverse primer CAAATTTTGCAGAGACTTTGGCACTG), yielding 465 and 552 bp fragments in the presence of the wild-type and mutant alleles, respectively. Heterozygous females have been crossed for at least 10 generations to C57BL/6J males to generate mutated males (*Pak3*-R67C knock-in mice) and littermate controls (WT). Different genotypes are generated at Mendelian ratio and heterozygous females and hemizygous males are fertile with no apparent phenotype.

Analysis of PAK3 mRNA expression by quantitative real-time PCR

Total RNA was isolated from adult brain using the TRIzol Reagent (Life Technologies) according to the manufacturer's protocol. The cDNA was generated from 0.5 µg of mRNAs using the iScript Reverse Transcription Supermix (Biorad). Real-time qPCR reactions were then run on a CFX96 Real-Time System C1000 Thermal Cycler (Bio-rad) using a Fast SYBR Green Master Mix kit (Applied Biosystems). The Pak3 primer set was obtained from Qiagen (QuantiTect Primer Assay: Mm_Pak3-1-SG; QT00119560) and used following the manufacturer's instructions. All samples were run in triplicates and normalized to HPRT1 and PGM1 expressions. The housekeeping genes Hprt1 and Pgm1 were chosen because their expression levels were comparable to that of the genes of interest. Data analysis was performed with the CFX Manager Software, 2.1 (Bio-rad), which incorporates the variability of data from both the housekeeping and target genes to calculate statistical significance. All samples were assayed in triplicate for each target or reference gene and the averaged values were used as Cycle Threshold (Cq). Changes in the relative expression of genes of interest (ΔCq) were calculated according to normalization to the endogenous controls PGK1 (Forward primer: 5'-

CTGACTTTGGACAAGCTGGACG -3' and Reverse primer: 5'- GCAGCCTTGATCCTTTGGTTG -3') and β2-Microglobulin (Forward primer: 5'- CCGCCTCACATTGAAATCCA -3' and Reverse primer: 5'- TCGATCCCAGTAGACGGTCTTG -3'), and then the ΔΔCq was calculated.

PAK3 protein expression in adult brain

Forebrains of two-month-old male mice were rapidly dissected, cut in small pieces with scalpel and homogenized with Dounce (10 pushes) in 10 volumes/weigh (i.e. 10 mL/1g) of cold lysis buffer containing 50 mM Tris-HCl, 1% Triton X-100, 100 mM NaCl, 50 mM NaF, 10 mM Na4P2O7, 5 mM EDTA, 1% aprotinin, 1 mM 4-(2-aminoethyl)-benzenesulfonylfluoride (Pefabloc SC, Interchim), pH 7.5, and then clarified by centrifugation (13.000 g, 10 min). Protein concentration in brain lysates were estimated by the Bradford method and aliquots of 25 µg of proteins were loaded in each lane and separated by SDS-polyacrylamide gel electrophoresis. PVDF-transferred proteins were detected with monoclonal antibodies, specific for PAK3 (Santa Cruz Biotechnology N19 Sc-1871) and β-Actin (Santa Cruz Biotechnology AC-15 Sc 69879). Quantification was assessed using a CCD camera (Fusion FX imaging system, Vilber Lourmat) and analysis was performed with ImageJ.

Generation of the *Pak3*-tm1b mice and analysis of PAK3 expression

The C57BL/6N-*Pak3*-tm1a(EUCOMM)Hmgu mice were generated at the ICS facility by injecting embryonic stem cell (ES) clones carrying the *Pak3* targeted allele (HEPD0663_5) obtained from the Knockout Mouse Project (KOMP) Repository into C57BL/6 blastocysts (25). Generation of *Pak3*-tm1b-lacZ reporter mice that express β-galactosidase under the control of endogenous *Pak3* promoter was obtained by crossing *Pak3*-tm1a mice with a global Cre deleter mouse expressing Cre recombinase ubiquitously under the control of a mouse Pgk1 promoter (56). This resulted in deletion of the neomycin cassette and critical exon 2, leading to the generation of tm1b-lacZ reporter mice that express β-galactosidase in cells where PAK3 would normally be expressed. Genotyping was performed by 3 primer-PCR with the following primers for Pak3-tm1a: 5'-GTGGGACTCTGACATCAATG-3, 5'-GCAGATAGGTACACACCAGC-3 and 5'-R 5'-CAACCTGACCTTGGGCAAGAAC, and for Pak3-tm1b : 985-MP3-E4-F 5'-

CCCATGGATACATAGCAGCAC, 5'-CTTATCATGTCGGATCCGG, and 5'-CACTTTGAAGACCAGACTGGTC. Analysis of PAK3 expression was done by β-galactosidase staining on tm1b brain slices. Briefly, brains were dissected as described below and free-floating brain sections (40 μm) were permeabilized for 10 min at room temperature in phosphate buffer containing 0.01% sodium-deoxycholate (w/v) and 0.02% Nonidet P-40 (v/v). Then, sections were stained with X-Gal reaction buffer (phosphate buffer containing 5 mM K3[Fe(CN)6], 5 mM K4[Fe(CN)6], 2 mM MgCl2) containing 0.8 mg/mL of X-Gal to visualize β-Gal activity. The reaction was performed overnight at 37°C in darkness. Subsequent to X-Gal staining, sections were washed in 0.1 M phosphate buffer for 10 min twice. After this staining, some sections were overnight at 4°C in a mouse anti-NeuN (1:100, MAB377, Millipore) and a guinea pig doublecortin (anti-DCX (1:4000, ab2253, Millipore). Sections were then incubated for two hours at room temperature in a goat anti-mouse IgG1 alexaFluor®488 (1:1000, a21121, Molecular Probes) and a goat anti-guinea pig alexaFluor®568 (1:500, a11075, Molecular Probes). Sections were mounted using Fluoromount medium.

Animal breeding

All the mice were housed in a temperature and light-controlled colony room (12-h light/dark cycle; 21 ± 1°C, 25 ± 5% humidity) in groups of 2-6 per cage with food and water ad libitum. Experiments were conducted during the light phase and performed blind to the genotype. Experimental procedures were conducted in accordance with the guidelines established by the European Communities Council Directive (2010/63/EU Council Directive Decree) and the Animal Experimentation Ethical Committee (CEEA N°59, project N°1408). All efforts were made to reduce the number of mice used and to minimize their suffering.

Irradiation procedure

One group of 8-week old male C57BL/6 wild-type mice were irradiated and tested in the delayed non-matching to place paradigm in the radial-arm maze (see below). Adult mice (n=10) were exposed to X-ray ionizing radiation using the Small Animal Radiation Research Platform (SARRP, Xstrahl, Ltd., UK) of IRSN (Fontenay-aux-Roses, France). The SARRP can deliver targeted radiation to preclinical

animal models with high accuracy (34). Using Cone Beam Computed Tomography (CBCT) from SARRP and magnetic resonance images recorded in parallel and manually superimposed on the SARRP treatment planning system (MuriPlan), the dorsal dentate gyrus was specifically irradiated with the protocol described in (34). Briefly, mice were anaesthetized by i.p. injection of a ketamine (100 mg/kg) / xylazine (10 mg/kg) solution. To irradiate all the dorsal dentate gyrus of adult mice, three isocenters were positioned and, for each, two beams at 180° to the sagittal plane were delivered using a circular 1 mm irradiation field. A fractioned protocol was used to give a total dose of 15 Gy (3 x 5 Gy spaced by 1 day). Throughout the duration of the study, there were no noticeable side effects of irradiation in terms of weight loss or hair loss. Non-irradiated sham control mice (NIR, n=8) were transported to the irradiation facility, anaesthetized, and subjected to the realization of CBCT images, but were not irradiated.

Behavioral procedures

Adult (3-month-old) male C57BL/6 *Pak3* hemizygous knock-in mice (*Pak3*-R67C, n=62) and Wild-Type (WT, n=78) littermate mice, distributed in 5 cohorts, were used in behavioral studies (supplementary table 1). Before the start of behavioral experiments, mice were handled 2 min per day for 3 days by the experimenter. For each behavioral task, a camera connected to a videotracking system (ANY-maze™, Stoelting) was placed above the devices to record behavioral sequences.

Open field study

One group of male *Pak3*-R67C (n=15) and WT littermate mice (n=12) aged 4 months was submitted to an open-field exploration test. The test arena was a square open-field (50 x 50 x 50 cm) with black walls and white floor under homogeneous illumination (100 lx in center area). Each mouse was released near the wall and allowed to move freely in the area during 40 min. X-Y positions were recorded to generate tracking plots of exploration paths and to calculate the distance traveled, time spent, average speed, and maximal speed (bouts of acceleration) in distinct zones of the arena (in the whole apparatus, in a 10-cm width virtual corridor along the walls and in the remaining center area). Latency of the first entry, number of entries, percent distance traveled in center area and along the

walls were calculated as relative measures of anxiety. Videos were analyzed offline using event-recorder keys in ANY-maze™ to quantify vertical activity (number of rearings/leanings).

Water maze set-up and training procedures

The water maze consisted of a circular tank (150 cm in diameter, 37 cm high) filled with water (21°C ± 0.5°C) to 7 cm below the top of the sidewall, made opaque by adding a white, non-toxic paint (Acusol OP301 Opacifier; Rohm and Haas). The maze was placed in a room containing several different cues on the walls. The pool was divided into four virtual quadrants. A circular escape platform (11.5 cm in diameter placed at 40 cm from the wall), submerged 0.5-cm below the water surface, was located in the center of one quadrant (target quadrant) and remained at a fixed location for each mouse during training. The three other quadrants served as starting points, assigned pseudo-randomly and varied on each trial. The maze was placed in a well-lit room (380 lx) containing several extra-maze cues. Data recorded by video-tracking (ANY-maze™) were used to reconstruct swim paths and to calculate averaged swim speed, swim path lengths and time spent in various virtual areas of the maze: the four quadrants, the four platform annuli (48-cm in diameter around the platform position) and a virtual corridor (19 cm in width) set along the wall to quantify thigmotaxis. Memory retention was evaluated during a probe test with the platform removed from pool. We compared the percent time spent in the quadrant that previously contained the platform to chance level (25%) and the number of crossings over the platform site in the quadrant that contained the platform during training.

Distributed protocol. One month after the open-field exploration test, a group of *Pak3*-R67C (n=15) and littermate WT mice (n=12) was submitted to a distributed spatial learning task in the water maze. One day before training, the mice underwent four trials of habituation during which they were trained to find and stay on the escape platform, placed in the center of the tank, for 60 s. Following habituation, the training phase lasted 11 days and consisted of 4 successive trials during which the platform was always located in the same quadrant for a given mouse. The position of the hidden platform was assigned for each mouse in one of the four virtual quadrants of the maze, such that the four positions were equally used in both groups of mice. Mice were introduced into the water maze

from three different starting points in the quadrants that did not contained the platform and were allowed to swim freely until reaching the platform. The sequence of starting points was chosen in a pseudorandom order and counterbalanced among individuals. Mice failing to find the platform after 90 s were gently guided to it by hand and a maximum escape latency of 90 s was recorded. Mice remained 60 s on the platform before the start of the next trial. After this training phase, a first probe test was performed 48h after the last training session and consisted of a single 90 s trial without platform. It was followed 1h later by one single trial in presence of the platform, to minimize extinction effects caused by the first probe trial. Another probe trial without platform was performed one week after the last training session.

Massed protocol. Another cohort of *Pak3*-R67C mice (n=6) and littermate WT mice (n=7) aged 3.5 months was used. For habituation, one day before training, the mice were submitted to a single habituation block of three trials, with the visible platform (protruding 0.5 cm above the water surface). A trial started by introducing the mouse into the maze facing the wall at one of the three designated starting points and allowed to swim freely until it reached the platform with a maximum time of 60 s. The mouse remained 60 s on the platform before being replaced at another starting point for the next trial. The next day, mice were trained to locate the hidden platform. The massed-training procedure (28) consisted in three training sessions separated by 2h, each composed of three blocks, 25-min apart, of three consecutive trials (27 trials in total). At each trial, a mouse was introduced into the maze from any of the three different starting points and allowed to swim freely until it reached the platform. If a mouse failed to find the platform after 60 s, it was gently guided to it and allowed to stay on it for 60 s before the start of the next trial. Ten days after learning, 2 successive 60 s probe tests, 3 min apart, are carried out.

Radial-arm maze set-up and training procedures

Three different types of behavioral tasks were performed in a radial maze with 3 different cohorts of mice. The device (Ugo Basile, Italy) consists of an octagonal central platform (diameter 16 cm) surrounded by 8 arms (35 cm long, 5.5 cm wide). At the end of each arm, small plastic cups (diameter

1 cm, 0.5 cm deep) are fixed to deposit a reward (20 µL of saccharin 0.1%) as a positive reinforcement. Doors at the entrance of each arm can be individually operated from a manual interface. The arms are open on the outside and allow the mouse to have a complete vision of extra-maze cues positioned on the walls of the testing room. One week prior to testing and during the training phase, mice were placed on a water-restriction regime. They had access to water for 10 min/day and maintained at 85-90% body weight during the entire duration of the experiment. During habituation, one day before training, the animals were habituated to the apparatus during two sessions. On the first session, a group of littermate mice was allowed to move freely in the maze and collect rewards during 5 min. On the second session, mice were individually placed in the maze for 5 min to retrieve rewards from the baited arm wells. The maze is cleaned with absolute alcohol between each mouse.

Working memory. In this elimination task, mice (WT n=10, *Pak3*-R67C n=11) had to recover rewards located at the end of the 8 arms of the radial maze without returning to a previously visited arm. Mice were submitted to 1 trial per day for 12 days. At the beginning of a trial, the mouse was placed in the center of the device surrounded by a transparent cylinder. All doors were open. The trial begins when the cylinder is removed. The maximum time for a trial is 5 min. If all rewards are recovered before the end of 5 minutes, the mouse is removed from the device. The number of working memory errors, consisting in entries into an already visited arm during a given trial, was counted.

Delayed non-matching to place paradigm in the radial-arm maze. The delayed non-matching to place (DNMP) paradigm was based on (29) and adapted in (7). During this task, WT (n=18) and *Pak3*-R67C (n=17) mice, aged 3.5 months, were tested. During training for 10 consecutive days, mice were submitted to 4 trials/day separated by 20 min. Each trial included two phases: a sample phase followed by a choice phase 20 s later (Fig. 3A). In the sample phase, only the start arm and one baited arm were opened. Once the reward was recovered, the mouse was removed from the maze, the maze was cleaned with alcohol and the choice phase started during which one additional arm was opened and was the only arm rewarded. This third arm varied in distance from the sample arm previously rewarded by either one arm (close configuration) or three arms (distant configuration; Fig. 3A). The

trial was considered successful if the mouse directly went to the novel rewarded arm. An error was counted if the mouse chose the sample arm as before. During the first two days of the experiment, mice had the opportunity to correct their errors by going to the rewarded arm. Every day, the mice were randomly submitted to 2 trials in close configuration and 2 trials in distant configuration. Each arm used (start, sample and test arms) during the trial alternate randomly. On day 11, a test was performed in which mice were submitted to 3 spaced trials of 3 min each, either in the close configuration (WT n=9, *Pak3*-R67C n=9) or in the distant configuration (WT n=9, *Pak3*-R67C n=8). The percentage of corrects choices was analyzed during training and test.

Successive spatial delayed non-matching to place in a radial-arm maze. To test memory flexibility and organization, and susceptibility to proactive interference, we used the task modeling declarative memory of repetitive everyday events developed by Abed et al. (33). This hippocampal-dependent task in the radial-arm maze requires the ability to retain recently visited places, i.e. which arm was the more recently visited within each of 3 repeatedly used pairs of arms, over varying intervals and intervening arm pairs. The task also requires the ability to organize and update the stored events as they are used, to overcome proactive interference from previous arm visits, and taxes both the retention and organizational components of hippocampus-dependent memory (33). We separately tested 2 cohorts of mice in this task: a group of WT (n=13) and *Pak3*-R67C (n=13) mice, and a group of irradiated (IR, n=10) and non-irradiated (NIR, n=8) mice. Two days before training, the animals were habituated to the apparatus during 4 sessions. The first day, the habituation protocol was similar to that of the previous behavioral task in the radial maze. The second day, mice were habituated to the opening / closing of the doors. For this, all arms were baited and each mouse was placed individually in the central platform with all arms closed. After 30 s, two or three arms were opened simultaneously and the mouse was allowed to get rewards, during 5 min. Training started the following day during 15 days. Each mouse was attributed a set of 3 pairs of adjacent arms (pairs a, b, and c; Fig. 4A) that were repeatedly and successively used until the end of training. At each training session, the mouse was submitted to successive presentations of the same 3 pairs, in a pseudo-random order, and required to choose the baited arm in each pair presentation. The position of the reward within each pair followed

an alternation rule, a natural mouse behavior. Thus, the reward was always positioned in the arm that was not visited by the mouse during the previous trial with the same pair (Fig. 4B). At the beginning of each daily session, the mouse was placed in the central platform with all arms closed. In the first trial with each pair, at the beginning of a training session, both arms contained a reward. Thus, this trial was just a "sampling" trial, not a "testing" trial, but then, the alternation rule applied and each trial becomes both a "testing" trial and a "sampling" trial. After 10 s, the mouse was given access to one of the 3 pairs of arms (a, b or c) and asked to choose to visit one of the 2 arms. The door of the non-chosen arm was closed as soon as the mouse reached the end of the chosen arm. As the mouse came back in the center, the door of the chosen arm was closed. After a fixed inter-trial interval of 10 s spent in the center, another trial began with 2 opened arms (same pair, or any of the other 2 pairs) and so on. Each daily session consisted of 23 trials with a 10 s inter-trial interval (ITI). Performance was measured as the percentage of correct trials over training and, for the last 3 days of training (days 13, 14, 15), as a function of the number of interfering trials (ITn) that corresponds to the number of trials with different pairs between 2 trials of the same pair. ITn can therefore vary from 0 (2 consecutive trials with the same pair) to 4 (4 interfering trials with different pairs between 2 trials from the same pair). The percentage of correct trials as a function of proactive interference (PI) was also calculated for the last 3 days of training. PI was dependent on the number of interfering trials between trial n and trial n-1 of the same pair. If the ITn between n-1 and n is small, the interference generated for the trial n+1 is more important and vice versa. Two categories of PI were analyzed, "low PI" for an ITn of 2 to 4 between trial n-1 and trial n, and "high PI" when the ITn is between 0 and 1 (Fig. 4B).

BrdU administration

To study adult newborn cell survival in basal conditions, *Pak3*-R67C and WT mice were given 3 BrdU injections (100 mg/kg, i.p.) at 4h intervals on a single day and were perfused 18 (*Pak3*-R67C n=5, WT n=5,), 28 (*Pak3*-R67C n=7, WT n=6,) or 38 (*Pak3*-R67C n=5, WT n=4) days later. To analyze cell survival after the spatial learning and memory task, a group of *Pak3*-R67C mice (n=6) and their littermate WT (n=7) received 3 i.p. injections of BrdU (100 mg/kg) at 4h intervals. The mice were then trained 18 days later and perfused 10 days after training (28 days after BrdU injections). To

quantify co-labeling with the immediate early gene Zif268, all mice were sacrificed 90 min after the end of the behavioral task. The control group without behavior testing corresponds to undisturbed mice remaining in their home cages and killed 28 days after BrdU injections (*Pak3*-R67C n=7, WT n=6, see above). Irradiated mice (IR n=10) and their non-irradiated controls (NIR n=8) received 2 BrdU injections per day (100 mg/kg, i.p.) at 8h intervals for 3 days and were trained 21 days later and perfused 15 days after the beginning of training (35 days after BrdU injections).

Preparation of tissue sections and Immunohistochemistry

Mice were deeply anaesthetized with an i.p. injection of pentobarbital (0.1%) and then perfused transcardially with a solution containing 4% cold paraformaldehyde (PFA) in 0.1M phosphate buffer (PB). Brains were dissected out and fixed overnight in PFA at 4°C, then transferred in PB 0.1M containing sucrose (10%, 20%, 30%), frozen in 2-methylbutane (−25°C) and preserved at -20°C. Coronal sections (40 µm) were cut with a cryostat and preserved in cryoprotectant solution. Revelations of $BrdU^+$, $Ki67^+$ and $NeuN^+$ cells were performed on floating sections. After several rinses in PBS (phosphate buffer solution) and PBS Triton X-100, the sections were immersed in a methanol solution (10%) and H_2O_2 (10%) to inactivate endogenous peroxidase. For BrdU revelation, two supplementary steps were made: the sections were placed in a solution of 2N HCl (30 min at 37°C) to denature the DNA strands and allow the antigenic sites to become accessible to the antibody and the pH was reduced to a neutral value with a boric acid bath (0.1M, 15 min, pH 8.5). After blocking antigenic sites with goat serum (5%), the sections were incubated overnight at 4°C in a rat anti-BrdU primary antibody (1:400, OBT0030, AbD Serotec), or a rabbit anti-Ki67 (1:400, ab16667 (SP6), Abcam), or a mouse anti-NeuN (1:600, MAB377, Millipore). Sections were then incubated in a goat biotinylated anti-rat (1:400, BA-9400, Eurobio), goat biotinylated anti-rabbit (1:400, BA-1000, Eurobio) or a goat biotinylated anti-mouse (1:400, BA-9200, Eurobio) secondary antibody for 1h30 at room temperature. Sections were then processed with avidin-biotin-peroxydase complex (1:400, ABC Elite Vector Labs) for 1h30, followed by three rinses of 5 min in PBS. The sections were then revealed in a DAB solution (3,3-diaminobenzidine-tetrahydrochloride; Sigma-Aldrich) to obtain black immunolabeling. Sections were then mounted on slides and stained-against Nuclear Fast Red in order

to visualize the GCL of the DG. After dehydration, the slides were mounted with the mounting medium (Eukitt).

Immunofluorescence

For BrdU or DCX double- and triple-labeling, sections treated as above were incubated overnight at room temperature in rat anti-BrdU (1:400, OBT0030, AbD Serotec) antibodies, together with the following antibodies: guinea-pig anti-DCX (1:1000, AB2253, Millipore) and/or mouse anti-NeuN (1:600, MAB377, Millipore), rabbit anti-GFAP (1:1000; DAKO), rabbit anti-Zif268 (1:100, (C-19):sc-189, Santa Cruz Biotechnology, inc), rabbit anti-glutamate receptor 1 (GluA1; 1:200; Millipore), rabbit anti-KCC2b (1:100; StressMarq Biosciences). Sections were then incubated for 1h30 at room temperature in goat biotinylated anti-rat (1:400, BA-9400, Eurobio) or a goat biotinylated anti-rabbit (1:400, BA-1000, Eurobio) antibodies followed by streptavidin alexaFluor®568 (1:1000; S11226, Invitrogen) or streptavidin alexaFluor®488 (1:1000; S11223, Invitrogen), or with anti-rabbit alexaFluor®488 (1:400, A11034, Invitrogen), anti-guinea pig alexaFluor®488 (1:400, A11073, Invitrogen), anti-mouse alexaFluor®647 (1:300, A21236, Invitrogen) and mounted in vectashield medium with DAPI (Vector Laboratories).

BrdU$^+$, Ki67$^+$ and DCX$^+$ cells quantification

All cell counts were conducted by an experimenter blind to the genotype and experimental conditions. Four to five mice per genotype were used. Labeled profiles were counted with an Olympus microscope (BX60) coupled with mapping software (MercatorPro; ExploraNova). The surface areas of the hippocampus, dentate gyrus and granule cell layer were traced in mapping software (Mercator Pro, Explora Nova), objective X10. Counting of BrdU$^+$ nuclei, Ki67$^+$ cells or DCX$^+$ cells was done only in DG of the dorsal hippocampus (bregma −1.15 mm to −3.30 mm). For BrdU quantification, 6 sections spaced by 240 µm were used per animal. For Ki67$^+$ and DCX$^+$ cells, 3 sections spaced by 480 µm were used per animal. The volume was determined by multiplying the surface area by the distance between sections (240 µm or 480 µm). Densities of BrdU$^+$, Ki67$^+$, and DCX$^+$ cells were estimated by multiplying the total number of labeled cells by 6 or by 12.

Double- and triple-labeling analysis and quantification

Sections were analyzed using the Zeiss confocal system (LSM700).

$BrdU^+$ cells: To establish the percentage of BrdU cells double-labeled with GFAP, or triple-labeled with NeuN and one of the following antibodies: DCX / Zif268 / GluA1 / KCC2b, 4-6 serial sections (240-µm spacing) from all mice were examined throughout the dorsal DG. Co-localizations were evaluated on 100-125 $BrdU^+$ cells per group of mice by performing z-stack acquisitions and 3D reconstructions to univocally verify double or triple labeling. All acquisitions were carried out in sequential scanning mode to prevent cross-bleeding between channels.

DCX^+ cells: To establish the percentage of DCX cells triple-labeled with Zif268 and NeuN, eight 10 µm stacks in 2 DG serial sections per mouse (two of each DG, 480-µm spacing) were collected at 40X. The number of $DCX^+/Zif268^+/NeuN^+$ cells in each stack was counted manually. In total, co-localizations were evaluated on 300-400 DCX^+ cells per group of mice.

$NeuN^+$ cells and $Zif268^+$ cells: To quantify the total number of cells in the GCL ($NeuN^+$ cells) and the percentage of $Zif268^+$ cells double-labeled with NeuN, twelve 6 µm stacks in 2 DG serial sections per mouse (six on each DG, 480-µm spacing) were collected at 40X. The number of $NeuN^+$ cells and $Zif268^+/NeuN^+$ cells in each stack was counted manually using Image J software (cells counters plugin) and summed per animal. In total, co-localizations were evaluated on 3800 $NeuN^+$ cells per group of mice.

Dendritic morphology analysis of DCX^+ cells

For morphological analysis of young neurons, we selected DCX^+ cells from infra- and suprapyramidal blades of the dorsal DG, with vertically orientated dendrites, extending through the molecular layer, and with, at least, tertiary dendritic branches (57, 58). Confocal images were acquired using a Zeiss LSM700 microscope with a X40 objective. For dendritic analysis, 3D reconstructions of the dendritic processes of each DCX^+ cell were made from sequential Z-stack images that were taken with 1 µm optical Z sections. The dendritic length and number of intersections were measured using the FIJI

image analysis software. Five mice from each genotype were analyzed with eight neurons from each mouse (n=40 from 5 mice per genotype).

Statistical Analysis

All data are presented as means ± SEM. For behavioral procedures (supplementary table 1), statistical comparisons were conducted by one-way or two-way with repeated measures ANOVAs. One-sample t-tests were used to compare performance against chance (25% in spatial memory tests; 50% in the successive spatial delayed non-matching to place task). For histochemical data, we used independent comparisons with Mann–Whitney non-parametric tests. Statistical tests were carried out using StatView 5.0 software. Significance level was set at $p < 0.05$.

Acknowledgments: This work was supported by the Centre National de la Recherche Scientifique (CNRS, France), the University Paris-Sud (France), the Fondation pour la Recherche sur le Cerveau [FRC 2013 grant to SL], the Jérôme Lejeune Foundation [Grant #1070 to JVB]; PHENOMIN (JVB) and ANR MRGENES to JVB and CV. CC and FD were supported by PhD fellowships from the French Ministry of Research, and LG by PhD fellowship from Fondation pour la Recherche Médicale (FRM, #ECO201806006842). The authors wish to thank the zootechnical platform in Orsay for animal breeding and care, Véronique Rousseau for her technical help; Bernadette Wiszniowski for genotyping; Morgane Dos Santos (IRSN, Research department in Radiobiology and regenerative MEDicine (SERAMED), Laboratory of Radiobiology of Accidental exposures (LRAcc, Fontenay-aux-Roses, France) and Gwennhael Autret (Small Animal Imaging Platform, Faculté de Médecine, Université Paris Descartes Sorbonne Paris Cité, Paris, France) for their help in the irradiation procedure; and Aline Marighetto (Neurocentre Magendie, Bordeaux, France) for advices and discussion on the successive spatial delayed non-matching to place task. M.C. Birling and M. Jaggla-Eberlin of the Mouse Clinical Institute (ICS, Illkirch) are acknowledged for technical support and discussions related to the generation of knock-in *Pak3*-R67C (IR2450) and *Pak3*-tm1a mice (IR5884),

and Karine Maillard from the TAAM (CNRS, Orleans) for providing us with the Cre-deleter mice. All authors declare no competing financial interests.

References

1 American Psychiatric Association. (2013) *Diagnostic and Statistical Manual of Mental disorders, fifth edition (DSM V)*. American Psychiatric Publishing, Book.

2 Vissers,L.E., Gilissen,C. and Veltman,J.A. (2016) Genetic studies in intellectual disability and related disorders. *Nat. Rev. Genet.,* **17**, 9-18.

3 Vaillend,C., Poirier,R. and Laroche,S. (2008) Genes, plasticity and mental retardation. *Behav. Brain. Res.*, **192**, 88–105.

4 van Bokhoven,H. (2011) Genetic and epigenetic networks in intellectual disabilities. *Annu. Rev. Genet.*, **45**, 81-104.

5 Pons-Espinal,M., De Lagran,M.M. and Dierssen,M. (2013) Functional implications of hippocampal adult neurogenesis in intellectual disabilities. *Amino Acids*, **45**, 113-131.

6 Allegra,M., Spalletti,C., Vignoli,B., Azzimondi,S., Busti,I., Billuart,P., Canossa,M. and Caleo,M. (2017) Pharmacological rescue of adult hippocampal neurogenesis in a mouse model of X-linked intellectual disability. *Neurobiol. Dis.*, **100** ,75-86.

7 Castillon,C., Lunion,S., Desvignes,N., Hanauer,A., Laroche,S. and Poirier,R. (2018) Selective alteration of adult hippocampal neurogenesis and impaired spatial pattern separation performance in the RSK2-deficient mouse model of Coffin-Lowry syndrome. *Neurobiol. Dis.,* **115**, 69-81.

8 Li,Y., Stockton,M.E., Eisinger,B.E., Zhao,Y., Miller,J.L., Bhuiyan,I., Gao,Y., Wu,Z., Peng,J. and Zhao,X. (2018) Reducing histone acetylation rescues cognitive deficits in a mouse model of Fragile X syndrome. *Nat. Commun.* **9**, 2494.

9 Sun,Y., Gao,Y., Tidei,J.J., Shen,M., Hoang,J.T., Wagner,D.F. and Zhao,X. (2019) Loss of MeCP2 in immature neurons leads to impaired network integration. *Hum. Mol. Genet*., **28**, 245-257.

10 Tzschach,A., Grasshoff,U., Beck-Woedl,S., Dufke,C., Bauer,C., Kehrer,M., Evers,C., Moog,U., Oehl-Jaschkowitz,B., Di Donato,N., et al. (2015) Next-generation sequencing in X-linked intellectual disability. *Eur. J. Hum. Genet.*, **23**, 1513–1518.

11 Hertecant,J., Komara,M., Nagi,A., Al-Zaabi,O., Fathallah,W., Cui,H., Yang,Y., Eng,C.M., Al Sorkhy,M., Ghattas,M.A., et al. (2017) A de novo mutation in the X-linked PAK3 gene is the underlying cause of intellectual disability and macrocephaly in monozygotic twins. *Eur. J. Med. Genet.*, **60**, 212-216.

12 Horvath,G.A., Tarailo-Graovac,M., Bartel,T., Race,S., Van Allen,M.I., Blydt-Hansen,I., Ross,C.J., Wasserman,W.W., Connolly,M.B. and van Karnebeek,C.D.M. (2018) Improvement of self-injury with dopamine and serotonin replacement therapy in a patient with a hemizygous PAK3 mutation: a new therapeutic strategy for neuropsychiatric features of an intellectual disability syndrome. *J. Child. Neurol.*, **33**, 106-113.

13 Kreis,P. and Barnier,J.V. (2009) PAK signalling in neuronal physiology. *Cell Signal.*, **21**, 384-393.

14 Bokoch,G.M. (2003) Biology of the p21-activated kinases. *Annu. Rev. Biochem.*, **72**, 743-781.

15 Boda,B., Alberi,S., Nikonenko,I., Node-Langlois,R., Jourdain,P., Moosmayer,M., Parisi-Jourdain,L. and Muller,D. (2004) The mental retardation protein PAK3 contributes to synapse formation and plasticity in hippocampus. *J. Neurosci.*, **24**, 10816-10825.

16 Hussain,N.K., Thomas,G.M., Luo,J. and Huganir,R.L. (2015) Regulation of AMPA receptor subunit GluA1 surface expression by PAK3 phosphorylation. *Proc. Natl. Acad. Sci. U S A,* **112,** 5883-5890.

17 Meng,J., Meng,Y., Hanna,A., Janus,C. and Jia,Z. (2005) Abnormal long-lasting synaptic plasticity and cognition in mice lacking the mental retardation gene Pak3. *J. Neurosci.*, **25**, 6641-6650.

18 Souopgui,J., Sölter,M. and Pieler,T. (2002) XPak3 promotes cell cycle withdrawal during primary neurogenesis in Xenopus laevis. *EMBO J.*, **21**, 6429-6439.

19 Maglorius Renkilaraj,M.R.L., Baudouin,L., Wells,C.M., Doulazmi,M., Wehrlé,R., Cannaya,V., Bachelin,C., Barnier,J.V., Jia,Z., Nait Oumesmar,B., et al. (2017) The intellectual disability protein PAK3 regulates oligodendrocyte precursor cell differentiation. *Neurobiol. Dis.*, **98**, 137-148.

20 Cobos,I., Borello,U. and Rubenstein,J.L. (2007) Dlx transcription factors promote migration through repression of axon and dendrite growth. *Neuron*, **54**, 873-388.

21 des Portes,V., Soufir,N., Carrié,A., Billuart,P., Bienvenu,T., Vinet,M.C., Beldjord,C., Ponsot,G., Kahn,A., Boué,J., et al. (1997) Gene for nonspecific X-linked mental retardation (MRX 47) is located in Xq22.3-q24. *Am. J. Med. Genet.,* **72**, 324-328.

22 Bienvenu,T., des Portes,V., McDonell,N., Carrie,A., Zemni,R., Couvert,P., Ropers,H.H., Moraine,C., van Bokhoven,H., Fryns,J.P., et al. (2000) Missense mutation in PAK3, R67C, causes X-linked nonspecific mental retardation. *Am. J. Med. Genet.*, **93**, 294-298.

23 Kreis,P., Thévenot,E., Rousseau,V., Boda,B., Muller,D. and Barnier,J.V. (2007) The p21-activated kinase 3 implicated in mental retardation regulates spine morphogenesis through a Cdc42-dependent 2 pathway. *J. Biol. Chem*., **282**, 21497-21506.

24 Allen,K.M., Gleeson,J.G., Bagrodia,S., Partington,M.W., MacMillan,J.C., Cerione,R.A., Mulley,J.C. and Walsh,C.A. (1998) PAK3 mutation in non syndromic X-linked mental retardation. *Nat. Genet.*, **20**, 25-30.

25 Skarnes,W.C., Rosen,B., West,A.P., Koutsourakis,M., Bushell,W., Iyer,V., Mujica,A.O., Thomas,M., Harrow,J., Cox,T., et al. (2011) A conditional knockout resource for the genome-wide study of mouse gene function. *Nature*, **474**, 337-342.

26 Jones,M.W., Errington,M.L., French,P.J., Fine,A., Bliss,T.V., Garel,S., Charnay,P., Bozon,B., Laroche,S. and Davis,S. (2011) A requirement for the immediate early gene Zif268 in the expression of late LTP and long-term memories. *Nat. Neurosci.*, **4**, 289-296.

27 Goodman,T., Trouche,S., Massou,I., Verret,L., Zerwas,M., Roullet,P. and Rampon,C. (2010) Young hippocampal neurons are critical for recent and remote spatial memory in adult mice. *Neuroscience*, **171**, 769-778.

28 Veyrac,A., Gros,A., Bruel-jungerman,E., Rochefort,C., Borgmann,F.B.K., Jessberger,S. and Laroche,S. (2013) Zif268/egr1 gene controls the selection, maturation and functional integration of adult hippocampal newborn neurons by learning. *Proc. Natl. Acad. Sci. U S A*, **110**, 7062–7067.

29 Clelland,C.D., Choi,M., Romberg,C., Clemenson,G.D., Fragniere,A., Tyers,P., Jessberger,S., Saksida,L.M., Barker,R.A. and Gage,F. (2009) A functional role for adult hippocampal neurogenesis in spatial pattern separation. *Science,* **325**, 210-213.

30 Winocur,G., Becker,S., Luu,P., Rosenzweig,S. and Wojtowicz,J.M. (2012) Adult hippocampal neurogenesis and memory interference. *Behav. Brain Res.*, **227**, 464-469.

31 Luu,P., Sill,O.C., Gao,L., Becker,S., Wojtowicz,J.M. and Smith,D.M. (2012) The role of adult hippocampal neurogenesis in reducing interference. *Behav. Neurosci.* **126**, 381-391.

32 Anacker,C. and Hen,R. (2017) Adult hippocampal neurogenesis and cognitive flexibility - linking memory and mood. *Nat. Rev. Neurosci.* **18**, 335-346.

33 Al Abed,A.S., Sellami,A., Brayda-Bruno,L., Lamothe,V., Noguès,X., Potier,M., Bennetau-Pelissero,C. and Marighetto,A. (2016) Estradiol enhances retention but not organization of hippocampus-dependent memory in intact male mice. *Psychoneuroendocrinology* **69**, 77-89.

34 Dos Santos,M., Kereselidze,D., Gloaguen,C., Benadjaoud,M., Tack,K., Lestaevel,P. and Durand,C. (2018) Development of whole brain versus targeted dentate gyrus irradiation model to explain low to moderate doses of exposure effects in mice. *Sci. Rep.*, **8**, 17262.

35 Meshi,D., Drew,M.R., Saxe,M., Ansorge,M.S., David,D., Santarelli,L., Malapani,C., Moore,H. and Hen,R. (2006) Hippocampal neurogenesis is not required for behavioral effects of environmental enrichment. *Nat. Neurosci.*, **9**, 729-731.

36 Kee,N., Teixeira,C.M., Wang,A.H. and Frankland,P.W (2007) Preferential incorporation of adult-generated granule cells into spatial memory networks in the dentate gyrus. *Nat. Neurosci.*, **10**, 355–362.

37 Trouche,S., Bontempi,B., Roullet,P. and Rampon,C. (2009) Recruitment of adult-generated neurons into functional hippocampal networks contributes to updating and strengthening of spatial memory. *Proc. Natl. Acad. Sci. U. S. A.,* **106**, 5919-5924.

38 Danielson,N.B., Kaifosh,P., Zaremba,J.D., Lovett-Barron,M., Tsai,J., Denny,C.A, Balough,E.M., Goldberg,A.R., Drew,L.J., Hen,R., et al (2016) Distinct Contribution of Adult-Born Hippocampal Granule Cells to Context Encoding. *Neuron,* **90**, 101-112.

39 Snyder,J.S., Clifford,M.A., Jeurling,S.I. and Cameron,H.A. (2012) Complementary activation of hippocampal-cortical subregions and immature neurons following chronic training in single and multiple context versions of the water maze. *Behav. Brain Res.*, **227**, 330-339.

40 Aasebø,I.E.J., Blankvoort,S., and Tashiro,A. (2011) Critical maturational period of new neurons in adult dentate gyrus for their involvement in memory formation. *Eur. J. Neurosci.*, **33**,1094-1100.

41 Hagihara,H., Ohira,K., Toyama,K. and Miyakawa,T. (2011) Expression of the AMPA receptor subunits GluR1 and GluR2 is associated with granule cell maturation in the dentate gyrus. *Front. Neurosci.*, **5**, 100.

42 Li,H., Khirug,S., Cai,C., Ludwig,A., Blaesse,P., Kolikova,J., Afzalov,R., Coleman,S.K., Lauri,S., Airaksinen,M.S., et al (2007) KCC2 interacts with the dendritic cytoskeleton to promote spine development. *Neuron,* **56,** 1019-1033.

43 Ge,S., Goh,E.L.K., Sailor,K.A., Kitabatake,Y., Ming,G., and Song,H. (2006) GABA regulates synaptic integration of newly generated neurons in the adult brain. *Nature*, **439**, 589-593.

44 Ming,G.L. and Song,H. (2011) Adult neurogenesis in the Mammalian brain: significant answers and significant questions. *Neuron*, **70**, 687–702.

45 Peippo,M., Koivisto,A.M., Sarkamo,T., Sipponen,M., von Koskull,H., Ylisaukko-oja,T., Rehnstrom,K., Froyen,G., Ignatius,J. and Jarvela,I. (2007) PAK3 related mental disability: Further characterization of the phenotype. *Am. J. Med. Genet. Part. A.*, **143**, 2406–2416.

46 Tronel,S., Belnoue,L., Grosjean,N., Revest,J.M., Piazza,P.V., Koehl,M. and Abrous,D.N. (2012) Adult-born neurons are necessary for extended contextual discrimination. *Hippocampus*, **22**, 292-298.

47 Nakashiba,T., Cushman,J.D., Pelkey,K.A., Renaudineau,S., Buhl,D.L., McHugh,T.J., Barrera,V.R., Chittajallu,R., Iwamoto,K.S., McBain,C.J., et al (2012) Young Dentate Granule Cells Mediate Pattern Separation, whereas Old Granule Cells Facilitate Pattern Completion. *Cell*, **149**, 188-201.

48 Saxe,M.D., Malleret,G., Vronskaya,S., Mendez,I., Garcia,A.D., Sofroniew,M.V., Kandel,E.R. and Hen,R. (2007) Paradoxical influence of hippocampal neurogenesis on working memory. *Proc. Natl. Acad. Sci. U S A,* **104**, 4642-4646.

49 Epp,J.R., Silva Mera,R., Köhler,S., Josselyn,S.A. and Frankland,P.W. (2016) Neurogenesis-mediated forgetting minimizes proactive interference. *Nat. Commun.*, **7**, 10838.

50 Aimone,J.B., Li,Y., Lee,S.W., Clemenson,G.D., Deng,W. and Gage,F.H. (2014) Regulation and Function of Adult Neurogenesis: From Genes to Cognition. *Physiol. Rev.*, **94**, 991–1026.

51 Gonçalves,J.T., Schafer,S.T. and Gage,F.H. (2016) Adult Neurogenesis in the Hippocampus: From Stem Cells to Behavior. *Cell*, **167**, 897-914.

52 Anacker,C. and Hen,R. (2017) Adult hippocampal neurogenesis and cognitive flexibility - linking memory and mood. *Nat. Rev. Neurosci.*, **18**, 335-346.

53 Sahay,A., Scobie,K.N., Hill,A.S. O'Carroll,C.M. Kheirbek,M.A. Burghardt,N.S., Fenton,A.A, Dranovsky,A. and Hen,R. (2011) Increasing adult hippocampal neurogenesis is sufficient to improve pattern separation. *Nature*, **472**, 466-470.

54 Vadodaria,K.C., Brakebusch,C., Suter,U. and Jessberger,S. (2013) Stage-specific functions of the small Rho GTPases Cdc42 and Rac1 for adult hippocampal neurogenesis. *J. Neurosci.*, **33**, 1179-1189.

55 Birling,M.C., Dierich,A., Jacquot,S., Hérault,Y. and Pavlovic,G. (2012) Highly-efficient, fluorescent, locus directed cre and FlpO deleter mice on a pure C57BL/6N genetic background. *Genesis*, **50**, 482-489.

56 Lallemand,Y., Luria,V., Haffner-Krausz,R. and Lonai,P. (1998) Maternally expressed PGK-Cre transgene as a tool for early and uniform activation of the Cre site-specific recombinase. *Transgenic Res.,* **7**, 105-112.

57 Pons-Espinal,M., Martinez,de Lagran, M.,Dierssen, M. (2013) Environmental enrichment rescues DYRK1A activity and hippocampal adult neurogenesis in TgDyrk1A. *Neurobiol. Dis.*, **60**, 18-31.

58 Chen,Q., Kogan,J.H., Gross,A.K., Zhou,Y., Walton,N.M., Shin,R., Heusner,C.L., Miyake,S., Tajinda,K., Tamura,K., Matsumoto,M. (2012) SREB2/GPR85, a schizophrenia risk factor, negatively regulates hippocampal adult neurogenesis and neurogenesis-dependent learning and memory. *Eur. J. Neurosci*. **36**, 2597-2608.

Legends to Figures

Figure 1. Generation of *Pak3*-R67C knock-in mice. (**A)** Targeting strategy for the knock-in of the PAK3-R67C mutation. After recombination and Cre-mediated loxP excision, the targeted allele contained the single nucleotide variation encoding the R67C missense mutation. (**B)** The R67C mutation suppresses a genomic *HhaI* restriction site in transgenic animals. High fidelity PCR-amplified fragments surrounding exon 2 were digested with *Hha* restriction enzyme and then analyzed by agarose electrophoresis. ND: non digested, D: *HhaI* digested sample, WT and R67C for wild type and hemizygous male mice, respectively. **(C)** The knock-in mutation does not modify protein expression. PAK3 protein expression from WT and *Pak3*-R67C (R67C) male adult brains was analyzed by western blot with PAK3 specific antibodies (upper band). Actin (lower band) was used as a control protein for normalization. Note that the signal level is similar for littermate WT and *Pak3*-R67C male mice. **(D)** Representative image of X-Gal deposit in hippocampal brain slices of *Pak3*-tm1b-lac Z reporter mice showing strong expression in mature neurons of CA1 layer and in the dentate gyrus. Scale bar = 200 µm. (**E**) NeuN immunoreactivity in WT and *Pak3*-R67C mice showing similar hippocampal structure. Scale bars = 200 µm.

Figure 2. Behavioral performance of *Pak3*-R67C mice in the distributed and massed spatial learning protocols in the water maze. (**A)** During distributed training, the latency to find the hidden platform declined similarly in WT (n=12) and *Pak3*-R67C mice (n=15). (**B**) 48h and (**C)** 1 week after acquisition, WT and *Pak3*-R67C mice spent significantly more time searching in the target quadrant compared with other quadrants. (**D)** During massed training, the latency to find the hidden platform declined similarly in WT (n=7) and *Pak3*-R67C mice (n=6). (**E**) Ten days after acquisition, WT mice spent significantly more time searching in the target quadrant compared with other quadrants, but not *Pak3*-R67C mice. (**F)** Mean number of crossings over the target location was significantly higher in WT than in *Pak3*-R67C mice. Error bars indicate SEM. * indicates significant differences between groups. # indicates significant difference compared to chance (25 %).

Figure 3. Behavioral performance of *Pak3*-R67C mice in the pattern separation task in the radial maze. (**A)** Pattern separation was tested using a DNMP protocol in the radial-arm maze by varying the distance (close or distant configurations) between the sample and correct arms. S, start arm; R, reward. Each trial consisted of a sample phase (left) and a choice phase (right). (**B)** Performance during 10 days of training was similar between WT (n=18) and *Pak3*-R67C (n=17) in both configurations. (**C)** On day 11, sub-groups of mice were submitted to 3 successive trials either in the close (WT n=9; *Pak3*-R67C n=9) or distant configuration (WT n=9; *Pak3*-R67C n=8). *Pak3*-R67C mice were impaired in the close but not in the distant configuration of the DNMP task. The horizontal black line represents chance. Error bars indicate SEM. * indicates significant differences between groups. # indicates significant difference compared to chance (50 %).

Figure 4. Behavioral performance of irradiated mice and of *Pak3*-R67C mice in the successive spatial DNMP task in the radial maze. (**A)** Radial maze with an example of a set of 3 pairs (a, b, c) of arms repeatedly used for a given mouse throughout memory testing in the successive spatial DNMP task. (**B**) An example of a sequence of trials within a session illustrating successive arm-pair presentations and arm-choices made by a mouse. Below are examples of selected trials illustrating the design to evaluate low and high proactive interference (see methods for details). (**C**) Percent correct choices increased progressively during training in non-irradiated (NIR, n=8) and irradiated (IR, n=10) mice. Performance of NIR mice was significantly above that of IR mice. (**D**) Performance during the last 3 training sessions (days 13, 14 and 15) as a function of the proximity between two identical trials. ITn, number of interfering trials. (**E**) Performance during the last 3 sessions (days 13, 14 and 15) as a function of the level of proactive interference (PI) for a given trial (Low PI, High PI) for NIR and IR mice. (**F)** Percent correct choices increased progressively during training in WT (n=13) and *Pak3*-R67C mice (n=13), however performance of WT mice was significantly above that of *Pak3*-R67C mice. (**G**) Performance during the last 3 training sessions (days 13, 14 and 15) as a function of the proximity between two identical tests. (**H**) Performance during the last 3 sessions (days 13, 14 and 15) as a function of the level of PI for a given trial (Low PI, High PI) for WT and *Pak3*-R67C mice. The

horizontal black line represents chance. Error bars indicate SEM. * indicates significant differences between groups. # indicates significant difference compared to chance (50 %).

Figure 5. Effect of the R67C mutation of the *Pak3* gene on basal adult hippocampal neurogenesis. (**A**) In the DG of *Pak3*-tm1b-lacZ reporter mice, *Pak3* promoter activity (lacZ staining in black) was stronger in the subgranular zone, in both mature ($NeuN^+$) and immature (DCX^+) neurons (upper images). Scale bars = 100 µm for left panel and 50 µm for right panel. **(B)** The density of $Ki67^+$ cells was similar between genotypes. (**C**) Total number of $BrdU^+$ cells at different days post injections (dpi). *Pak3*-R67C mice showed significantly less $BrdU^+$ cells than WT mice at 28 dpi. (**D**) The density of DCX^+ cells was not significantly different between genotypes. (**E**) The percentage of $BrdU^+$ cells expressing DCX and / or NeuN was similar between genotypes at the 3 different dpi. (**F**) Representative confocal images of 18-day-old $BrdU^+$ newborn cells expressing DCX and NeuN in the DG from a WT mouse. Scale bars = 10 µm. For each point, four to five mice per genotype were used. Data are means ± SEM. * indicates significant differences between groups.

Figure 6. Effect of spatial learning and recall on adult-born hippocampal neurons in *Pak3*-R67C mice. (**A**) Mice received 3 injections of BrdU on day 0 (D0), were submitted to spatial learning in the water maze on day 18 (D18) and to retention test 10d later (D28). (**B)** As in the basal condition (Home Cage Controls, HC CTRL; Fig. 5C), the density of 28-day-old $BrdU^+$ cells after recall was significantly lower in *Pak3*-R67C mice than in WT mice, but the spatial behavioral task had no significant impact on survival of newly born 28-day-old $BrdU^+$ neurons in either genotype. (**C**,**D**,**E**) Analysis of Zif268-expressing dentate gyrus neurons of different ages following recall. (**C)** Percentage of DCX^+ dentate granule cells expressing Zif268 upon recall is increased in WT mice, but there is a complete failure of recruitment of young DCX^+ newborn neurons in *Pak3*-R67C mice. (**D)** Upon spatial memory recall, the number of $BrdU^+/NeuN^+$ DGCs expressing Zif268 was identical in WT and *Pak3*-R67C mice. (**E)** Percentage of $NeuN^+$ DGCs expressing Zif268 increased after recall in both WT and *Pak3*-R67C mice with no significant difference between genotypes. For each point, four to five mice per genotype were used. Data are means ± SEM. * indicates significant differences between groups.

Figure 7. Effect of the R67C mutation of the *Pak3* gene on KCC2b expression in newborn cells of *Pak3*-R67C mice. (**A**) The percentage of 18-day-old newborn BrdU$^+$ DGCs expressing KCC2b was lower in *Pak3*-R67C (n=5) than in WT (n=5) mice. (**B**) Confocal micrographs of 18-day-old newborn BrdU$^+$ cells expressing KCC2b in a WT mouse. White and yellow arrows indicate BrdU$^+$ DGCs expressing or not KCC2b. Scale bars = 10 µm. (**C**) DCX immunostaining in the dorsal DG from *Pak3*-R67C and WT mice (scale bar = 100 µm for left panel and 20 µm for right panel), and representative 3D dendritic morphology of DCX$^+$ cells from a WT and a *Pak3*-R67C mouse. (**D-E**) Morphological analysis of DCX$^+$ cells. (**D**) Total dendritic length of DCX$^+$ cells and (**E**) Dendritic branching numbers were significantly reduced in *Pak3*-R67C compared to WT mice. Eight neurons per mouse and five mice per genotype were analysed. * indicates significant differences between genotypes.

Supplementary figure 1. General behavioral characterization of *Pak3*-R67C mice. (**A**) Total distance traveled over 40 min in an open-field in WT (n=12) and *Pak3*-R67C (n=15) mice. (**B**) Vertical activity (number of rearings) in the open-field. (**C**) Percentage of time spent in the central zone of the open-field. (**D**) Percentage of correct choices over 11 days of training in the working memory task in the 8-arm radial maze in WT (n=10) and *Pak3*-R67C (n=11) mice. Error bars indicate SEM.

Supplementary figure 2. Swim speed and thigmotaxis of *Pak3*-R67C mice in the distributed and massed spatial learning protocols in the water maze. (**A**) During distributed training, the average swim speed was slightly higher as training progressed in *Pak3*-R67C mice (n=15) compared to WT mice (n=12). (**B**) Thigmotaxis significantly decreased over training in WT and *Pak3*-R67C mice. (**C**) During massed training, the average swim speed was identical between WT (n=7) and *Pak3*-R67C mice (n=6). (**D**) Thigmotaxis decreased significantly for WT and *Pak3*-R67C mice during training. Error bars indicate SEM.

Supplementary figure 3. Targeted irradiation of the dorsal dentate gyrus significantly reduced the number of dentate gyrus newborn neurons in irradiated (IR) mice. (A) Effect of irradiation on

the density of 35 day-old $BrdU^+$ cells and **(B)** of immature DCX^+ newborn neurons in the dorsal DG. (**C**) Representative microphotographs illustrating DCX labeling in the dorsal DG of non-irradiated (NIR) and irradiated (IR) mice. Scale bar = 100 µm. (**D**) The targeted irradiation of the dorsal DG had no significant impact on the density of immature DCX^+ newborn neurons in the ventral DG from IR mice. Error bars indicate SEM. * indicates significant differences between groups.

Supplementary table 1: Statistical analyses of performance in behavioral tasks

Abbreviations

ANOVA: Analysis of variance

AMPA: Amino-3-hydroxy-5-methyl-4-isoxazolepropionic acid

BAC: Bacterial Artificial Chromosome

BrdU: 5-Bromo-2-deoxyUridine

CBCT: Cone Beam Computed Tomography

Cdc42: Cell division control protein 42

cDNA: complementary Deoxyribonucleic Acid

CREB: cAMP-Response Element Binding protein

Cq: Cycle Threshold

DAB: 3,3- diaminobenzidinetetrahydrochloride

DAPI: 4',6-diamidino-2-phénylindole

DCX: Doublecortin

DG: Dentate Gyrus

DGC: Dentate Granule Cell

DNA: Deoxyribonucleic Acid

DNMP: Delayed Non-Matching to Place

Dpi: days post injections

ES cell: Embryonic Stem cell

GABA: Acide γ-Aminobutyrique

GCL: Granule Cell Layer

GFAP: Glial Fibrillary Acidic Protein

GluA: Glutamate receptor

GTPase: Guanosine Triphosphate hydrolase

HCl: Hydrochloric acid

HC-CTRL: Home Cage Control mice

H*haI*: restriction enzyme

HPRT1: Hypoxanthine Phosphoribosyltransferase 1

ID: Intellectual Disability

ITI: Inter-Trial Interval

ITn: Interfering Trials number

IR: Irradiated

KCC2b: K^+Cl^- Co-transporter 2b

LIMK: LIM kinase

MAP Kinase: Mitogen-Activated Protein Kinases

NeuN: Neuronal Nuclei

NIR: Non-Irradiated

Pak3: p21-activated kinase-3

Pak3-R67C mouse: mouse of the *Pak3*-dependent ID model bearing the R67C missense mutation

Pak3-tm1a mouse: mouse generated by injecting embryonic stem cell (ES) clones carrying the Pak3-targeted allele ((HEPD0663_5) (EUCOMM nomenclature)

Pak3-tm1b-lac Z reporter mouse: mouse that expresses β-galactosidase under the control of the endogenous Pak3 promoter

PB: Phosphate Buffer

PCR: Polymerase Chain Reaction

PFA: Paraformaldehyde

PGM1: Phosphoglucomutase 1

PGK1: Phosphoglycerate Kinase 1

PI: Proactive Interference

PVDF: Polyvinylidene difluoride

qPCR: quantitative Polymerase Chain Reaction

Rac1: Ras-related C3 botulinum toxin substrate 1

RNA: Ribonucleic Acid

RT-PCR: Reverse Transcription Polymerase Chain Reaction

TRIzol : guanidinium thiocyanate

WT: Wild-Type

Zif268: Zinc Finger transcription Factor 268

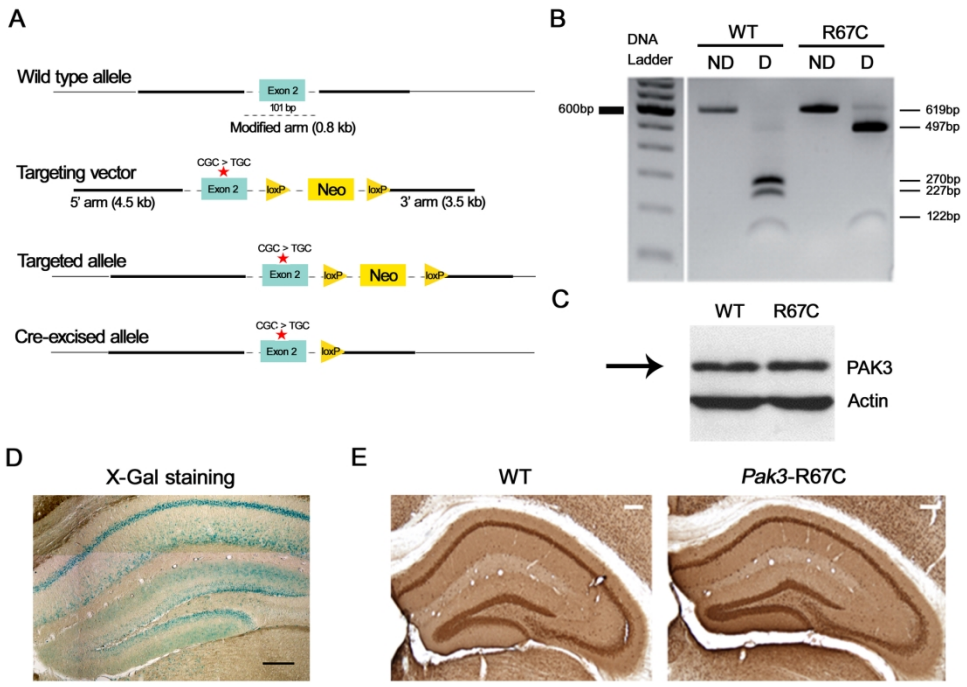

Figure 1. Generation of Pak3-R67C knock-in mice. (A) Targeting strategy for the knock-in of the PAK3-R67C mutation. After recombination and Cre-mediated loxP excision, the targeted allele contained the single nucleotide variation encoding the R67C missense mutation. (B) The R67C mutation suppresses a genomic HhaI restriction site in transgenic animals. High fidelity PCR-amplified fragments surrounding exon 2 were digested with Hha restriction enzyme and then analyzed by agarose electrophoresis. ND: non digested, D: HhaI digested sample, WT and R67C for wild type and hemizygous male mice, respectively. (C) The knock-in mutation does not modify protein expression. PAK3 protein expression from WT and Pak3-R67C (R67C) male adult brains was analyzed by western blot with PAK3 specific antibodies (upper band). Actin (lower band) was used as a control protein for normalization. Note that the signal level is similar for littermate WT and Pak3-R67C male mice. (D) Representative image of X-Gal deposit in hippocampal brain slices of Pak3-tm1b-lac Z reporter mice showing strong expression in mature neurons of CA1 layer and in the dentate gyrus. Scale bar = 200 µm. (E) NeuN immunoreactivity in WT and Pak3-R67C mice showing similar hippocampal structure. Scale bars = 200 µm.

170x120mm (300 x 300 DPI)

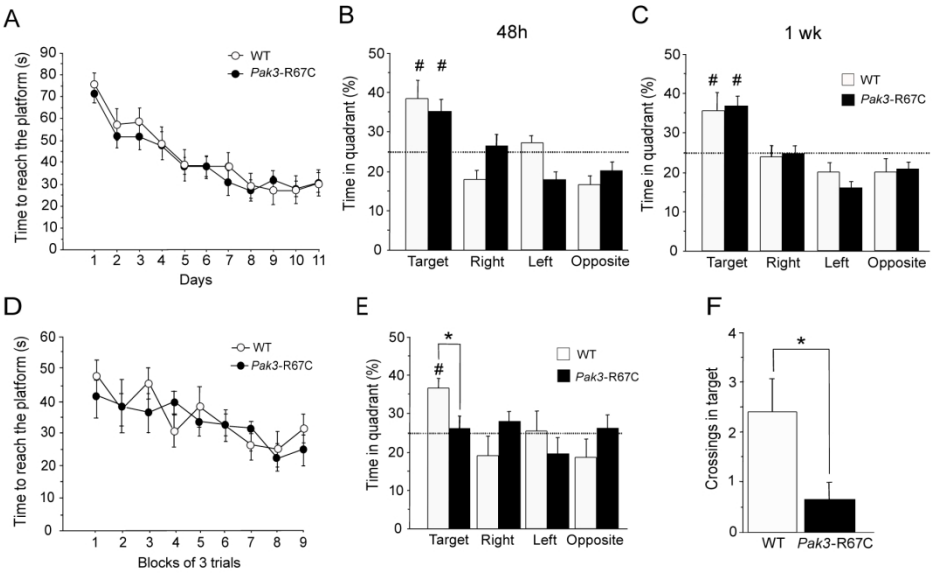

Figure 2. Behavioral performance of Pak3-R67C mice in the distributed and massed spatial learning protocols in the water maze. (A) During distributed training, the latency to find the hidden platform declined similarly in WT (n=12) and Pak3-R67C mice (n=15). (B) 48h and (C) 1 week after acquisition, WT and Pak3-R67C mice spent significantly more time searching in the target quadrant compared with other quadrants. (D) During massed training, the latency to find the hidden platform declined similarly in WT (n=7) and Pak3-R67C mice (n=6). (E) Ten days after acquisition, WT mice spent significantly more time searching in the target quadrant compared with other quadrants, but not Pak3-R67C mice. (F) Mean number of crossings over the target location was significantly higher in WT than in Pak3-R67C mice. Error bars indicate SEM. * indicates significant differences between groups. # indicates significant difference compared to chance (25 %).

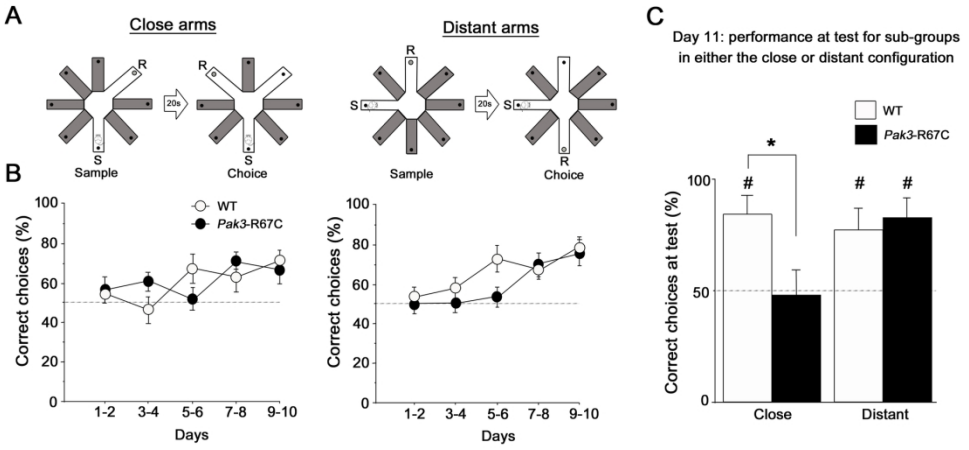

Figure 3. Behavioral performance of Pak3-R67C mice in the pattern separation task in the radial maze. (A) Pattern separation was tested using a DNMP protocol in the radial-arm maze by varying the distance (close or distant configurations) between the sample and correct arms. S, start arm; R, reward. Each trial consisted of a sample phase (left) and a choice phase (right). (B) Performance during 10 days of training was similar between WT (n=18) and Pak3-R67C (n=17) in both configurations. (C) On day 11, sub-groups of mice were submitted to 3 successive trials either in the close (WT n=9; Pak3-R67C n=9) or distant configuration (WT n=9; Pak3-R67C n=8). Pak3-R67C mice were impaired in the close but not in the distant configuration of the DNMP task. The horizontal black line represents chance. Error bars indicate SEM. * indicates significant differences between groups. # indicates significant difference compared to chance (50 %).

170x80mm (300 x 300 DPI)

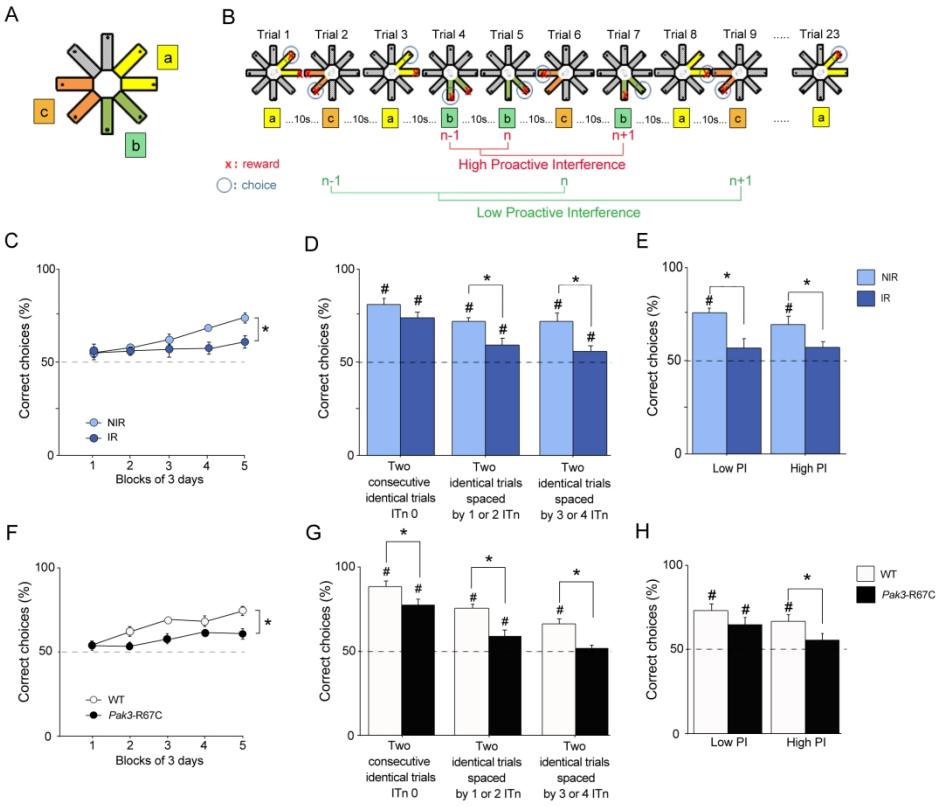

Figure 4. Behavioral performance of irradiated mice and of Pak3-R67C mice in the successive spatial DNMP task in the radial maze. (A) Radial maze with an example of a set of 3 pairs (a, b, c) of arms repeatedly used for a given mouse throughout memory testing in the successive spatial DNMP task. (B) An example of a sequence of trials within a session illustrating successive arm-pair presentations and arm-choices made by a mouse. Below are examples of selected trials illustrating the design to evaluate low and high proactive interference (see methods for details). (C) Percent correct choices increased progressively during training in non-irradiated (NIR, n=8) and irradiated (IR, n=10) mice. Performance of NIR mice was significantly above that of IR mice. (D) Performance during the last 3 training sessions (days 13, 14 and 15) as a function of the proximity between two identical trials. ITn, number of interfering trials. (E) Performance during the last 3 sessions (days 13, 14 and 15) as a function of the level of proactive interference (PI) for a given trial (Low PI, High PI) for NIR and IR mice. (F) Percent correct choices increased progressively during training in WT (n=13) and Pak3-R67C mice (n=13), however performance of WT mice was significantly above that of Pak3-R67C mice. (G) Performance during the last 3 training sessions (days 13, 14 and 15) as a function of the proximity between two identical tests. (H) Performance during the last 3 sessions (days 13, 14 and 15) as a function of the level of PI for a given trial (Low PI, High PI) for WT and Pak3-R67C mice. The horizontal black line represents chance. Error bars indicate SEM. * indicates significant differences between groups. # indicates significant difference compared to chance (50 %).

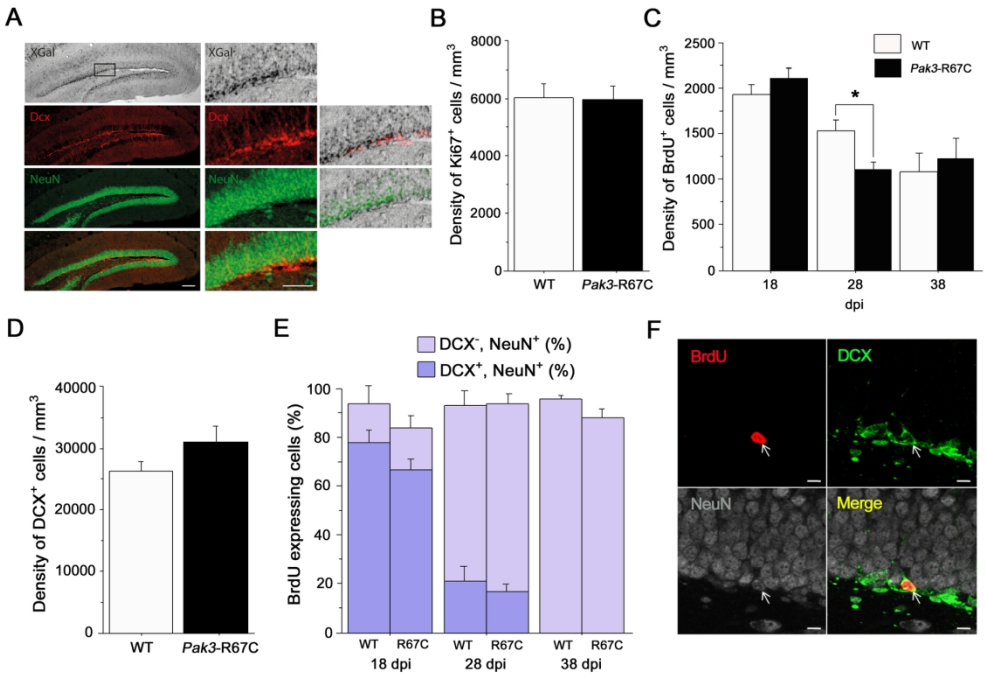

Figure 5. Effect of the R67C mutation of the Pak3 gene on basal adult hippocampal neurogenesis. (A) In the DG of Pak3-tm1b-lacZ reporter mice, Pak3 promoter activity (lacZ staining in black) was stronger in the subgranular zone, in both mature (NeuN+) and immature (DCX+) neurons (upper images). Scale bars = 100 µm for left panel and 50 µm for right panel. (B) The density of Ki67+ cells was similar between genotypes. (C) Total number of BrdU+ cells at different days post injections (dpi). Pak3-R67C mice showed significantly less BrdU+ cells than WT mice at 28 dpi. (D) The density of DCX+ cells was not significantly different between genotypes. (E) The percentage of BrdU+ cells expressing DCX and / or NeuN was similar between genotypes at the 3 different dpi. (F) Representative confocal images of 18-day-old BrdU+ newborn cells expressing DCX and NeuN in the DG from a WT mouse. Scale bars = 10 µm. For each point, four to five mice per genotype were used. Data are means ± SEM. * indicates significant differences between groups.

170x120mm (300 x 300 DPI)

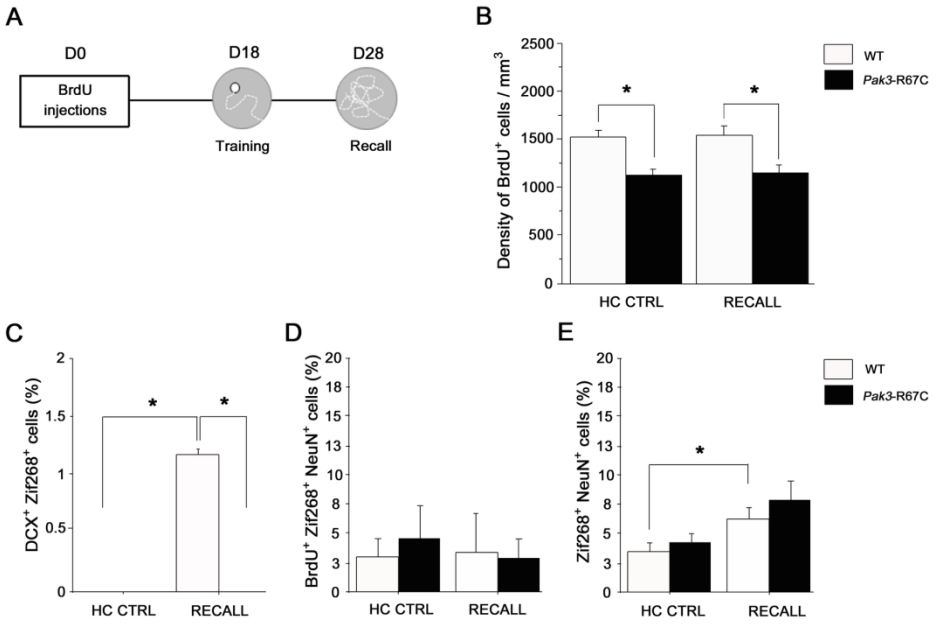

Figure 6. Effect of spatial learning and recall on adult-born hippocampal neurons in Pak3-R67C mice. (A) Mice received 3 injections of BrdU on day 0 (D0), were submitted to spatial learning in the water maze on day 18 (D18) and to retention test 10d later (D28). (B) As in the basal condition (Home Cage Controls, HC CTRL; Fig. 5C), the density of 28-day-old BrdU+ cells after recall was significantly lower in Pak3-R67C mice than in WT mice, but the spatial behavioral task had no significant impact on survival of newly born 28-day-old BrdU+ neurons in either genotype. (C,D,E) Analysis of Zif268-expressing dentate gyrus neurons of different ages following recall. (C) Percentage of DCX+ dentate granule cells expressing Zif268 upon recall is increased in WT mice, but there is a complete failure of recruitment of young DCX+ newborn neurons in Pak3-R67C mice. (D) Upon spatial memory recall, the number of BrdU+/NeuN+ DGCs expressing Zif268 was identical in WT and Pak3-R67C mice. (E) Percentage of NeuN+ DGCs expressing Zif268 increased after recall in both WT and Pak3-R67C mice with no significant difference between genotypes. For each point, four to five mice per genotype were used. Data are means ± SEM. * indicates significant differences between groups.

170x120mm (300 x 300 DPI)

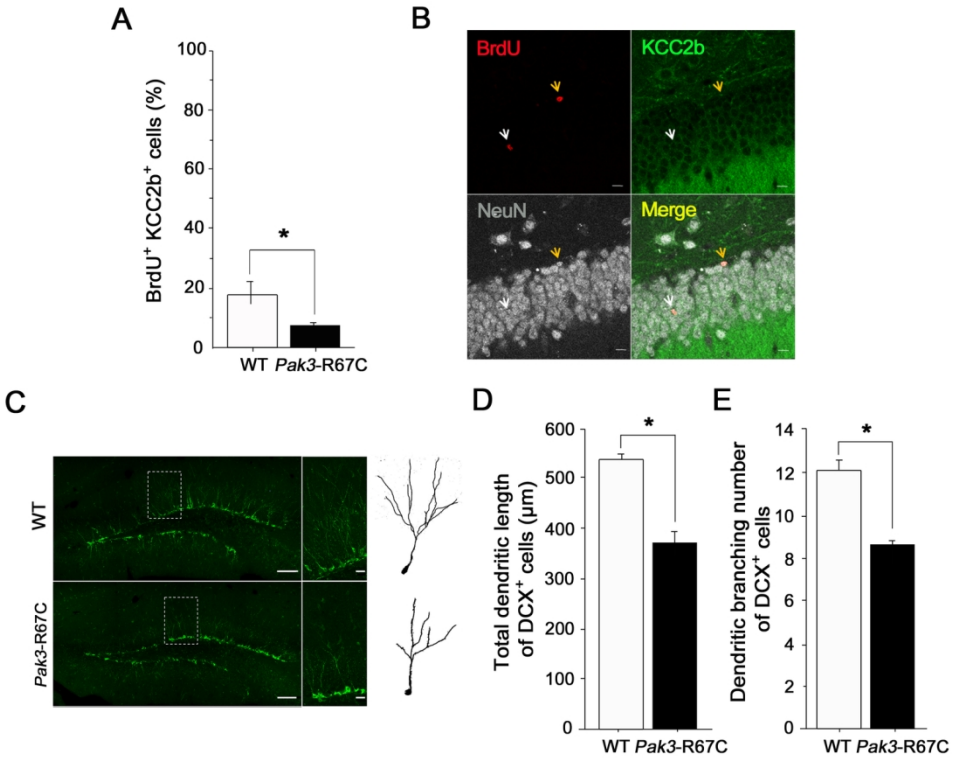

Figure 7. Effect of the R67C mutation of the Pak3 gene on KCC2b expression in newborn cells of Pak3-R67C mice. (A) The percentage of 18-day-old newborn BrdU+ DGCs expressing KCC2b was lower in Pak3-R67C (n=5) than in WT (n=5) mice. (B) Confocal micrographs of 18-day-old newborn BrdU+ cells expressing KCC2b in a WT mouse. White and yellow arrows indicate BrdU+ DGCs expressing or not KCC2b. Scale bars = 10 µm. (C) DCX immunostaining in the dorsal DG from Pak3-R67C and WT mice (scale bar = 100 µm for left panel and 20 µm for right panel), and representative 3D dendritic morphology of DCX+ cells from a WT and a Pak3-R67C mouse. (D-E) Morphological analysis of DCX+ cells. (D) Total dendritic length of DCX+ cells and (E) Dendritic branching numbers were significantly reduced in Pak3-R67C compared to WT mice. Eight neurons per mouse and five mice per genotype were analysed. * indicates significant differences between genotypes.

140x110mm (300 x 300 DPI)

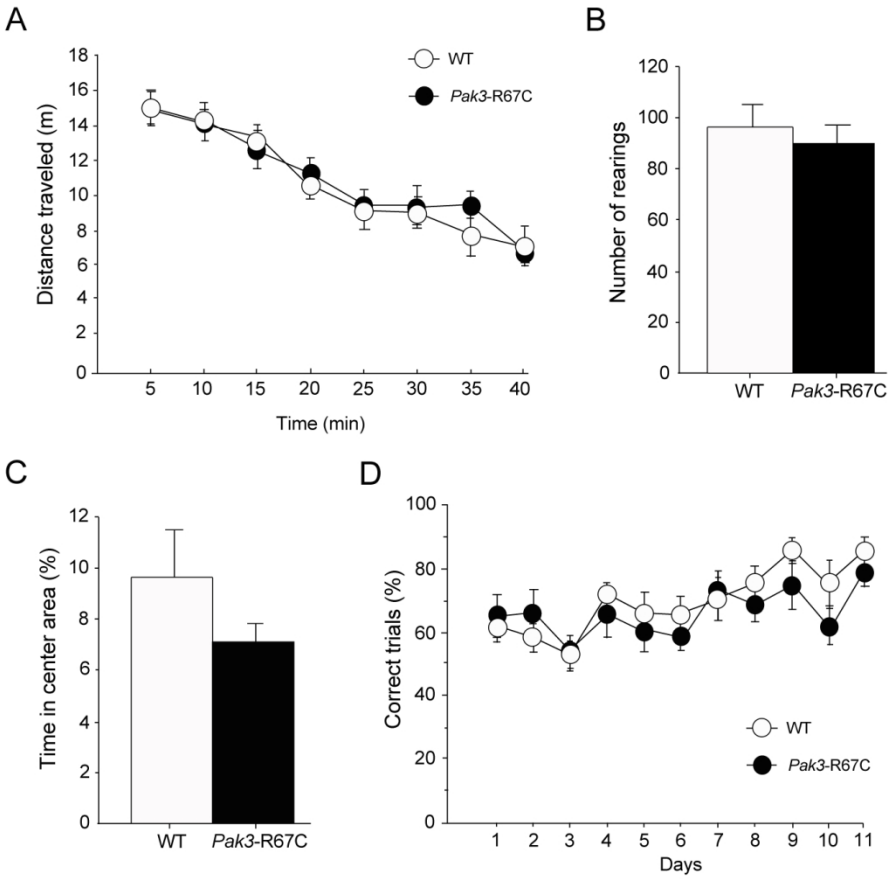

Supplementary figure 1. General behavioral characterization of Pak3-R67C mice. (A) Total distance traveled over 40 min in an open-field in WT (n=12) and Pak3-R67C (n=15) mice. (B) Vertical activity (number of rearings) in the open-field. (C) Percentage of time spent in the central zone of the open-field. (D) Percentage of correct choices over 11 days of training in the working memory task in the 8-arm radial maze in WT (n=10) and Pak3-R67C (n=11) mice. Error bars indicate SEM.

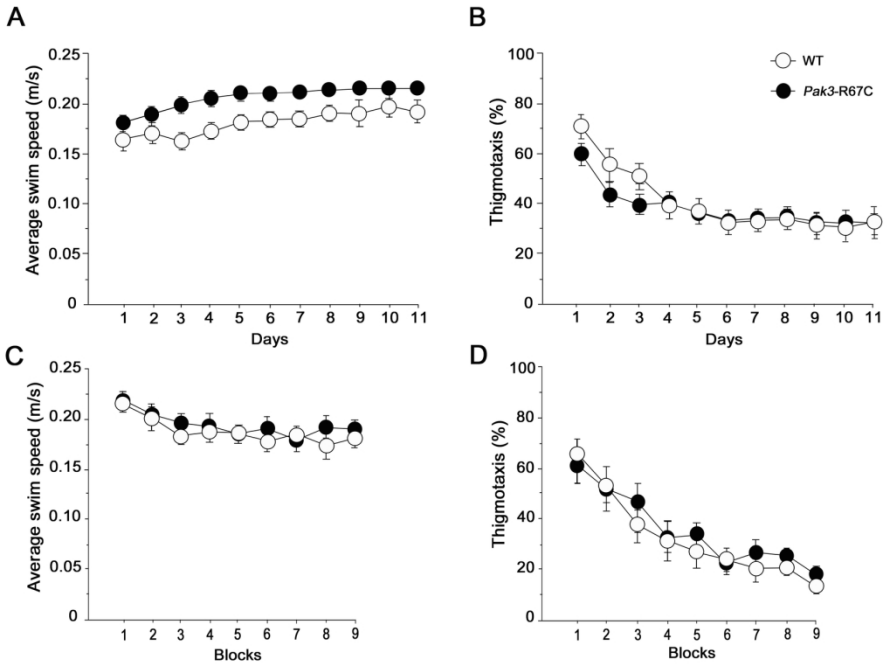

Supplementary figure 2. Swim speed and thigmotaxis of Pak3-R67C mice in the distributed and massed spatial learning protocols in the water maze. (A) During distributed training, the average swim speed was slightly higher as training progressed in Pak3-R67C mice (n=15) compared to WT mice (n=12). (B) Thigmotaxis significantly decreased over training in WT and Pak3-R67C mice. (C) During massed training, the average swim speed was identical between WT (n=7) and Pak3-R67C mice (n=6). (D) Thigmotaxis decreased significantly for WT and Pak3-R67C mice during training. Error bars indicate SEM.

160x120mm (300 x 300 DPI)

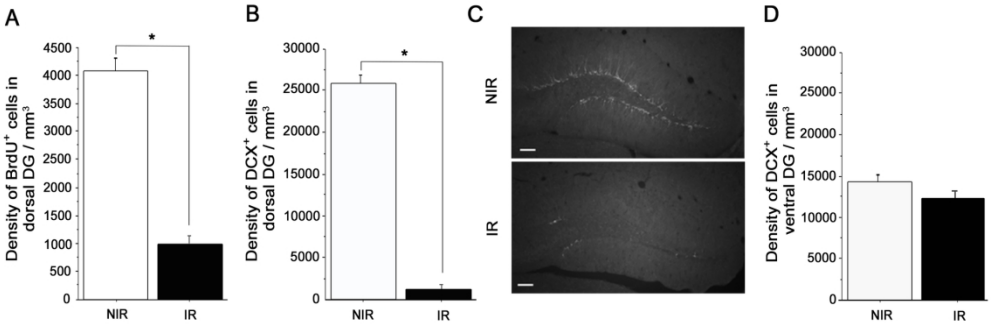

Supplementary figure 3. Targeted irradiation of the dorsal dentate gyrus significantly reduced the number of dentate gyrus newborn neurons in irradiated (IR) mice. (A) Effect of irradiation on the density of 35 day-old BrdU+ cells and (B) of immature DCX+ newborn neurons in the dorsal DG. (C) Representative microphotographs illustrating DCX labeling in the dorsal DG of non-irradiated (NIR) and irradiated (IR) mice. Scale bar = 100 μm. (D) The targeted irradiation of the dorsal DG had no significant impact on the density of immature DCX+ newborn neurons in the ventral DG from IR mice. Error bars indicate SEM. * indicates significant differences between groups.

170x60mm (300 x 300 DPI)